scientific reports

Check for updates

OPEN

The potential of the South African plant *Tulbaghia Violacea* Harv for the treatment of triple negative breast cancer

Mohammed Alaouna[1,6], Thulo Molefi[2,6,8], Richard Khanyile[2,8], Nkhensani Chauke-Malinga[3,6,8], Aristotelis Chatziioannou[4,6,8], Thifhelimbilu Emmanuel Luvhengo[5,6], Maropeng Raletsena[6,7], Clement Penny[1,6], Rodney Hull[6,8]✉ & Zodwa Dlamini[6,8]✉

Triple-negative breast cancer (TNBC) is difficult to treat and has a low five-year survival rate. In South Africa, a large percentage of the population still relies on traditional plant-based medicine. To establish the utility of both methanol and water-soluble extracts from the leaves of *Tulbaghia violacea*, cytotoxicity assays were carried out to establish the IC_{50} values against a TNBC cell line. Cell cycle and apoptosis assays were carried out using the extracts. To identify the molecular compounds, present in water-soluble leaf extracts, NMR spectroscopy was performed. Compounds of interest were then used in computational docking studies with the anti-apoptotic protein COX-2. The IC_{50} values for the water- and methanol-soluble extracts were determined to be 400 and 820 µg/mL, respectively. The water-soluble extract induced apoptosis in the TNBC cell line to a greater extent than in the normal cell line. RNAseq indicated that there was an increase in the transcription of pro-apoptotic genes in the TNBC cell line. The crude extract also caused these cells to stall in the S phase. Of the 61 compounds identified in this extract, five demonstrated a high binding affinity for COX-2. Based on these findings, the compounds within the extract show significant potential for further investigation as candidates for the development of cancer therapeutics, particularly for TNBC.

Keywords Apoptosis induction, Cell cycle regulation, Computational docking, COX-2, Cytotoxicity assays, Molecular compound isolation, Traditional plant-based medicine, Triple negative breast cancer (TNBC), *Tulbaghia Violacea*

Abbreviations

AB	Alamar Blue
Aas	Amaryllidaceae alkaloids
CDKs	Cyclins and cyclin-dependent kinases
COX-2	Cyclooxygenase 2 protein
DDMP	3-dihydro-3,5-dihydroxy-6-methyl
DFS	Disease-free survival
DMSO	Dimethyl sulfoxide

[1]Department of Internal Medicine, Faculty of Health Sciences, University of the Witwatersrand, Johannesburg, South Africa. [2]Department of Medical Oncology, Steve Biko Academic Hospital, University of Pretoria, Pretoria 0001, South Africa. [3]Papillon Aesthetics, Suite 302b Netcare Linksfield Hospital, 24 12th Ave, Linksfield West, Johannesburg 2192, South Africa. [4]Center of Systems Biology, Biomedical Research Foundation of the Academy of Athens, Athens 11527, Greece. [5]Department of Surgery, Charlotte Maxeke Johannesburg Academic Hospital, University of the Witwatersrand, Parktown, Johannesburg 2193, South Africa. [6]Department of Chemical pathology, Faculty of Health Sciences, University of the Witwatersrand, Johannesburg, South Africa. [7]Department of Chemistry, University of South Africa, Florida Campus, Johannesburg, South Africa. [8]SA-MRC Precision Oncology Research Unit (PORU), DSTI/NRF SARChI Chair in Precision Oncology and Cancer Prevention (POCP), Pan African Cancer Research Institute (PACRI), University of Pretoria Hatfield, Pretoria 0028, South Africa. ✉email: Rodney.hull@up.ac.za; Zodwa.Dlamini@up.ac.za

5FU	5-fluorouracil
GMP	Guanosine monophosphate
NMR	Nuclear Magnetic Resonance
OS	Overall survival
PANTHER	Protein Analysis THrough Evolutionary Relationships
PI	Propidium iodide
ROS	Reactive oxygen species
RTCA	Real-Time Cell Analysis
TNBC	Triple -negative breast cancer
UMP	Uridine monophosphate

Triple-negative breast cancer (TNBC) is an aggressive form of breast cancer that has a high risk of spreading. A tenth to a twentieth of all incidences of breast cancer are caused by the faulty cellular mutations that give rise to TNBC[1]. These mutations result in downregulated or absent expression of the receptors for progesterone, estrogen, and human epidermal growth factor receptor 2 on the surface of breast cancer cells[2]. As a result, TNBC is difficult to treat, being immune to hormone therapy. The disease also has a high recurrence rate, and these factors contribute to TNBC patients having a poor overall survival rate[3,4]. Since TNBC subtypes account for 15–20% of all breast cancers, the number of cases is around 170,000 worldwide[4–7]. TNBC risk factors differ slightly from those for many other subtypes of breast cancer. Decreased lifelong sensitivity to testosterone, long periods of breastfeeding, and being younger when giving birth to their first child will generally provide protection against hormone-positive breast cancer. In contrast to this, the prevalence of TNBC has been found to be negatively associated with a longer period of breastfeeding[8–11]. TNBC has an earlier onset age, with the majority of TNBC cases being diagnosed and treated by the age of thirty-nine[12]. Another important risk factor that is of particular importance in Africa is the role played by ethnicity in TNBC. Despite the fact that they have a lower overall breast cancer risk than white women, African American women die at a higher rate[13] and have a higher incidence of TNBC than white women. Additionally, black women tend to be diagnosed with TNBC at a younger age[8,14].

Patients with TNBC are treated with non-specific cytotoxic multi-agent chemotherapy. The effectiveness of these treatments have been clinically demonstrated[15]. Despite their dismal prognosis, TNBC tumors are particularly chemo sensitive, albeit for a shorter duration than other breast cancers. Polychemotherapy, including the favorable effect of taxane-containing regimens on various disease-associated factors such as the risk of recurrence, disease-free survival (DFS), and overall survival (OS) in TNBC, has been shown to be effective in several trials[16–18].

Plants contain non-nutritive bioactives, a diverse group of organic chemicals known as phytochemicals[19]. Recently, phytochemicals isolated from green plants that have previously been used for medicinal purposes have become the focus of the hunt for new cancer-preventative and cancer-therapeutic compounds[20]. Surprisingly, plants are the source of 47% of FDA-approved medications that may be used to treat cancer. The Madagascar periwinkle (Catharanthus roseus) is a crucial source of the anti-cancer drugs vinblastine and vincristine, which are extracted in very low concentrations, approximately 0.0002–0.0005% by weight[21]. These alkaloids are significant due to their potent anti-cancer properties, particularly in treating various malignancies, including lymphomas and solid tumors[22]. Recent research has focused on enhancing the yield and efficacy of these compounds through synthetic modifications and biotechnological approaches, aiming to overcome the limitations associated with their low natural abundance[23,24].

While several of these plant extracts have been explored as anti-cancer drugs in clinical trials, only a few affect biochemical or molecular pathways that are actively involved in cancer and tumor formation and regulation, including cell cycle inhibitors, mitogenic signaling antagonists (growth and proliferation), metastasis inhibitors, and immune system receptors[25]. One of the most common modes of action for phytochemicals in the treatment of cancer is through the induction or modulation of autophagy and apoptosis[26–28].

Tulbaghia violacea (T. violacea) Harv. (Amaryllidaceae) is a tiny bulbous plant native to South Africa. The plant is exclusively found in South Africa, namely in the provinces of Natal, Gauteng, Northwest, Limpopo, Mpumalanga, and the Eastern Cape. The leaves are hairless and grow on a slender, fleshy stem[29]. Infusions in water using *Tulbaghia violacea*(wild garlic) have been used in traditional medicine in Southern Africa to cure a variety of ailments, including treating the symptoms associated with a variety of cancers. Many previous studies using this plant have indicated that it may have verifiable effects on tumor cells. In these studies it was shown that organic solvent extracts of *T. violacea* been shown to induce apoptosis in various cancer cell lines accompanied by the overexpression of p53[30–32]}. Other studies have indicated that water-soluble extracts induce apoptosis through increased caspase expression. The extracts were also shown to be selective for cancer cells, inducing cell death in these cells at a higher rate than in normal cells[32].

Although *T. violacea* has been used in traditional medicine to treat various ailments, very little scientific research has been done to validate these uses. This study involved creating water- and methanol-soluble extracts from the leaves of *T. violacea* and testing their ability to kill cancer cells, specifically TNBC cells. This also involved establishing IC_{50} values for these crude extracts, which would allow for the use of relevant concentrations in further tests of the anti-cancer nature of these extracts.

Materials and methods

Preparation of plant extracts

Plant extracts of *T. violacea* were prepared using aqueous and methanol based extractions to obtain a water-soluble and a non-water-soluble extract. The species of the collected plant material used in this study was collected from Garden Goods CC, located in Johannesburg, South Africa (PO Box 68859, Bryanston, 2021).

The collection was conducted in February during the summer season, as seasonal variations can influence the phytochemical composition of Tulbaghia violacea. plants were confirmed by the staff at the C. E. Moss Herbarium at the University of the Witwatersrand, and the specimen was cataloged under the reference number CEM-TULB-2019-215, ensuring the authenticity of the plant material used in the study. The leaves of the plant were collected, rinsed with water, and, cut and dried for 120 h at 40 °C, a process that is critical for preserving the integrity of the bioactive compounds[33]. The plant material was finely ground and passed through an 850-micron sieve. The extraction of the water-soluble compounds was performed by dissolving 100 g of dry powder in 1 L of boiled water and allowed to cool for 24 h before filtering. This method is consistent with traditional aqueous extraction techniques that maximize the yield of hydrophilic compounds[34]. The methanol extraction was performed by dissolving 100 g of dried powder in 250 mL of pure methanol. The filtrate was placed in a Soxhlet extractor for 72 h. This technique is well-documented for its efficiency in extracting a wide range of bioactive compounds from plant materials[35]. Both extracts were freeze dried to obtain a dry powder, a process that helps in preserving the bioactive properties of the extracts[36]. Aqueous extracts were created by dissolving the powder in a sufficient quantity of either physiological saline, deionized water, or cell culture media. Methanol extracts were created by dissolving powder in either physiological saline, de-ionized water, or culture media containing less than 0.5% of DMSO to enhance solubility[37]. The stock was then dissolved to the final test concentrations by dissolving the stock in serum-free culture media. The diluted extract was applied to cells for 24 h in fresh culture medium containing 10% FBS.

Cell culture

This study utilized MCF-10 A (normal human mammary gland epithelial cells) and MDA-MB-231 (human mammary cancer cells) cell lines. The MCF-10 A cell line was donated by Professor Raquel Duarte (University of the Witwatersrand, Department of Internal medicine). The MCF-10 A cell line was cultured in DMEM/F12 media with 5% horse serum, 20 ng/mL EGF, 0.5 µg/mL hydrocortisone, 100 ng/mL cholera toxin, 10 µg/mL insulin, and 1% penicillin/streptomycin[38]. The MDA-MB-231 cell line was revived from frozen stocks (stored in liquid Nitrogen) and initially purchased from ATCC (HTB-26). The MDA-MB-231 cell line was cultured in DMEM high glucose media with 10% FBS and 1% penicillin/streptomycin. The MDA-MB-231 cell line is cultured in DMEM high glucose media with 10% FBS and 1% penicillin/streptomycin.

Cytotoxicity assays

Assay for cell viability with Alamar Blue (AB)

Alamar blue, also known as resazurin, is widely used to determine cell viability due to its non-toxic nature and effectiveness in various biological applications[39,40]. Cells were cultured as previously described in a 96-well plate. The cells were serum-starved for 24 h to synchronize the cell cycle. Different concentrations of plant extracts were used to treat the cultured cells (100, 200, 300, 400, 500, and 600 ug/mL), with a 0.2% DMSO control. Untreated controls consisted of cells grown in regular tissue culture media. Cells incubated with 5FU served as a positive control. Cells were left for 48 h to grow in the presence of the treatments. Following this, the media was removed and replaced with fresh media with a 10% concentration of Alamar Blue. The cells were incubated for 4 h. The absorbance of the plates was then read on a Spectromax ABS + plate reader (molecular devices). The percentage of viable cells expressed as a percentage of AB reduction as a function of dye strength was calculated using the formula.

$$\%\ \text{Reduction of Alamar Blue Reagent} = \frac{(\text{Eoxi600} \times \text{A570}) - (\text{Eoxi570} \times \text{A600}) \times 100}{(\text{Ered570} \times \text{C600}) - (\text{Ered600} \times \text{C570})}$$

Where:

A600 = absorbance of test wells at 600 nm.

Eoxi570 = molar extinction coefficient (E) of oxidized Alamar Blue Reagent at 570 nm = 80,586.

Eoxi600 = E of oxidized Alamar Blue Reagent at 600 nm = 117,216.

A570 = absorbance of test wells at 570 nm[41].

The Alamar Blue assay is recognized for its versatility and reliability in various biological applications, including cytotoxicity testing and cell viability assessments[42]. It operates on the principle of cellular reduction of resazurin to resorufin, which can be quantitatively measured, thus providing a clear indication of cell metabolic activity[43]. Moreover, the assay's non-toxic nature allows for continued experimentation with the same cell population after viability assessment, which is a significant advantage in experimental design[44]. Recent studies have optimized the Alamar Blue assay to enhance its replicability and reproducibility, further solidifying its role in cancer drug sensitivity screens[39].

Determination of IC50 values using real-time cell analysis

The xCELLigence Real-Time Cell Analysis (RTCA) system was used to establish the IC_{50}.

Value of both extracts. Varying concentrations of the plant extracts (0, 50, 150, and 350 ug/mL) were used to treat the cells. In addition to this, a vehicle control for the methanol extracts was added to two wells. The cells were grown on the e-16 plate while being monitored by the RTCA device for 24 h before treatment. The extracts, DMSO, or drug were added to each appropriate well at a final volume of 200 uL of media per well. A kinetic record of the cells was generated after treating them with different amounts of plant extract, offering essential insights about the cells' biological condition, particularly cell viability. A figure correlating cell viability with the logarithm of chemical concentration was created using data obtained from cell impedance. The IC_{50} values for each crude extract were determined using the RTCA program.

The RTCA system's ability to continuously monitor cell viability and proliferation makes it an invaluable tool for determining cytotoxicity, as it eliminates the need for cell termination and labeling, which are common in other assays[45–47]. This method has been shown to provide dynamic intermediary cytotoxicity data that cannot be delivered in endpoint assays, thereby enhancing the accuracy of IC50 determinations (Ülker et al., 2021). Studies indicate that DMSO can have varying effects on different cell types, and it is essential to include appropriate controls to assess its cytotoxicity[48,49].

Analyzing the ability of the active plant extract to induce apoptosis in TNBC and normal breast cells

In order to determine if the active plant extract is able to induce apoptosis, the percentage of treated cells undergoing apoptosis was determined using the Muse™ Annexin V & Dead Cell Kit (Merck (MCH100105)[50]. Five different populations of cells were cultured separately. One population served as the untreated control, while one served as a positive control for cell death. The remaining three populations were treated with the IC_{50} concentration of *T. violacea* water extract, a concentration of water extract slightly lower than the IC_{50}, and a final concentration of plant extract higher than the IC_{50}. Cultured cells were serum-starved for 24 h and then treated with the relevant compounds for 48 h. The plant extracts were dissolved in standard culture medium. Both the untreated control and the positive control were not treated. After 48 h, the positive control cells were removed, centrifuged, and the cell pellet was immersed in boiling water to eliminate the cells. The other cell samples were also detached, and all pellets were resuspended in 1% FBS in 1X Assay Buffer HSC (CatLog No. 4700–325). The cell suspension and the annexin V and dead cell reagent were mixed in a 1:1 ratio (100 uL of each). This cell mixture was incubated for 20 min before analyzing the Annexin V and dead cell programs on the Muse instrument. The analysis was calibrated using a positive control consisting of heat-killed cells. The percentage of live, early apoptotic cells and the percentage of late apoptotic and dead cells for each cell population were recorded and plotted as a bar graph of the percentage of cells in each population.

Analyzing the effect of the active plant extract on the progression of the cells through the cell cycle

In order to determine the effects of active plant extracts on the ability of treated cells to progress through the cell cycle, the DNA content was determined using flow cytometry and propidium iodide (PI) staining[51]. Cyclins and cyclin-dependent kinases (CDKs) regulate cell cycle progression, while checkpoints regulate the cell's entry into each phase[52]. The cells were treated as before with three different concentrations of *T. violacea* water-soluble extract. One concentration below the IC_{50}, one above the IC_{50}. After 48 h, the cells were harvested and fixed in ice-cold absolute ethanol. The fixed cells were then rehydrated and treated with RNAse at 37 °C to remove the RNA[53]. The cells were then stained with a 1 mg/mL solution of PI (1 mg/mL) and incubated at 4 °C overnight in the dark. The labelled cells were subsequently examined using the cell cycle analysis feature on the Muse flow cytometer.

The use of flow cytometry in this context is well-established, as it allows for the precise measurement of cellular DNA content, which is essential for assessing cell cycle progression[51]. The regulation of the cell cycle by cyclins and CDKs is a fundamental concept in cell biology, where specific cyclins activate corresponding CDKs to facilitate transitions between different phases of the cell cycle[52]. Moreover, the treatment with T. violacea extract at varying concentrations provides insight into its potential cytotoxic effects, which can be evaluated by analyzing the changes in DNA content and cell cycle distribution[54]. Recent studies have highlighted the importance of understanding how plant extracts can influence cell cycle dynamics, particularly in the context of stress responses and disease resistance in plants[55]. The methodology involving PI staining is particularly effective for distinguishing between viable and non-viable cells, as PI penetrates only cells with compromised membranes, thus allowing for the assessment of cell viability and apoptosis[56].

In summary, the analysis of the effects of *T. violacea* water-soluble extract on cell cycle progression involves a systematic approach utilizing flow cytometry and PI staining to evaluate DNA content and cell viability. This methodology is supported by a robust understanding of cell cycle regulation mechanisms and the implications of extract concentration on cellular responses. Furthermore, the exploration of phytochemicals in plant extracts has been shown to induce cell cycle arrest and apoptosis in various cancer cell lines, emphasizing their potential as therapeutic agents[57,58].

Determining the molecular composition of the water-soluble extract

NMR spectroscopy

The NMR tube was cleaned using a method described by Zhang et al.[59]., and about 10 mg the freeze-dried water-soluble extract of Tulbaghia violacea leaves was added. All of the substance was dissolved before the sample was gently shaken. To guarantee that all of the sample was exposed to a uniform magnetic field, the spinner was turned after it was placed in the magnet. In order to get rid of fingerprints and grime, 2-propanol and lab tissues were used to wipe the exterior of the NMR tube. The rotor, an autosampler-equipped Varian 600 MHz spectrometer, was employed. After the NMR test was completed, the spectrum was analyzed, and the peaks were assigned. An NMR spectrum's interpretation was performed using an appropriate application to analyze the spectrum (MestReNova)[60].

Computational modelling of the interaction of COX – 2 and components of the T. violacea water soluble extract

T. violacea bioactive compounds identified by NMR analysis were chosen and used to search for protein docking targets using the High-Throughput Docking website. The protein most commonly found in all searches with the highest average docking score was the Cyclooxygenase 2 protein (COX-2). The 3D X-ray crystal structure of the protein was retrieved from the Protein Data Bank, we opted to focus on chain A only for both COX-1 (6Y3C)

and COX-2 (5IKT), because it represents the functional monomer most commonly used in drug discovery and docking studies. (Fig. 1A,B). The proteins and ligands were prepared using the Protein Preparation Wizard (Schrödinger, Inc) and LigPrep processing in the Schrödinger Suite. The initial nine compounds derived from *Tulbaghia violacea* water extracts was expanded to sixteen due to the generation of chemically plausible variations

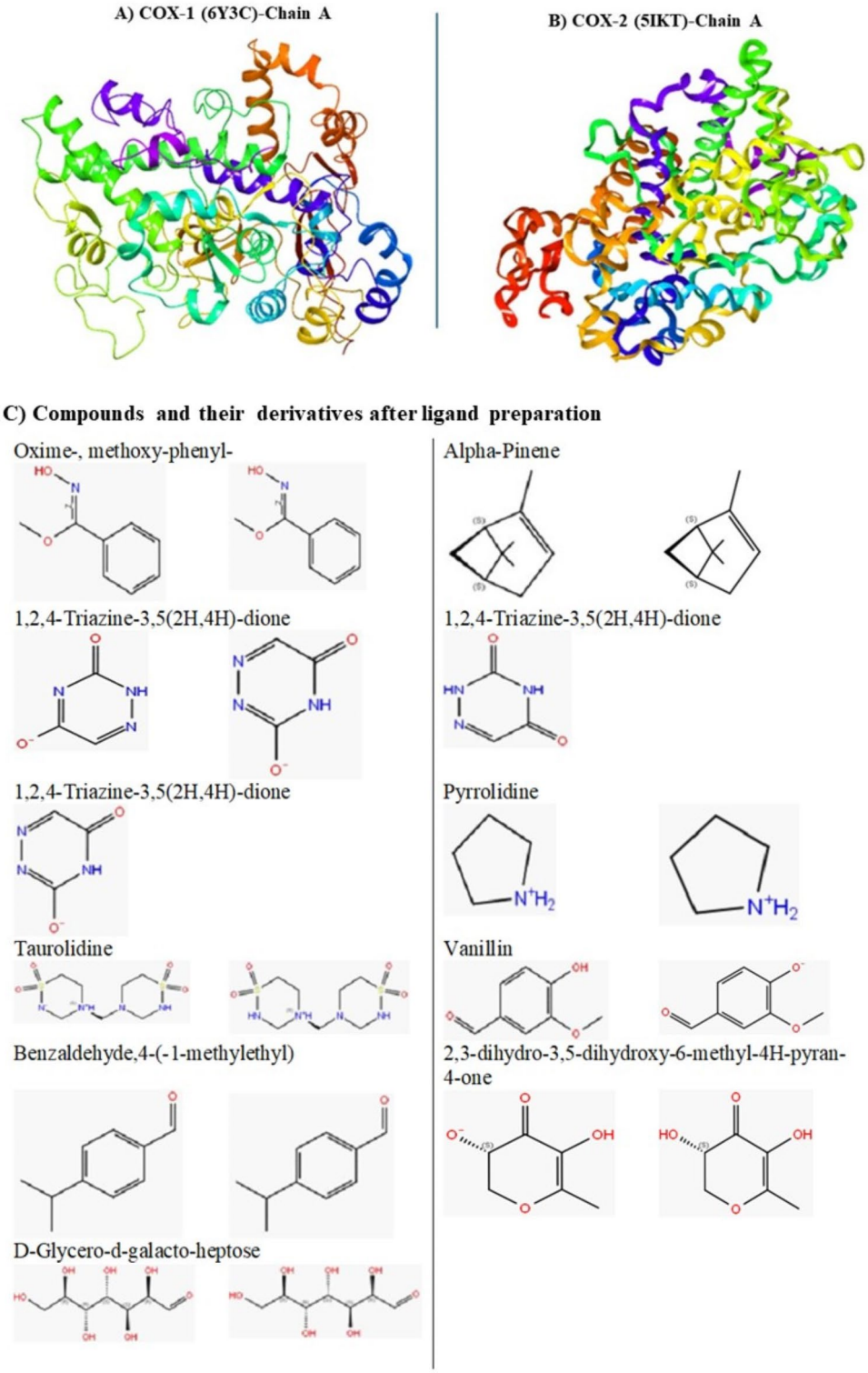

Fig. 1. The molecules used in the docking analysis. (**A**) The protein target COX-1 and (**B**) COX-2. (Protein Databank, www.rcsb.org). (**C**) Structure of compounds identified from *T. violacea* and used for the molecular docking.

through tautomerization, protonation state adjustments, and stereoisomer enumeration. Sitemap analysis was performed to identify notable differences in the binding site characteristics of COX-1 and COX-2.

Sitemap_Cox1_site_5 and sitemap_Cox2_site_2 were selected for the docking comparison. Docking analysis was performed using Maestro Schrödinger Suite 2024-3. Standard Precision (SP) docking was performed to rapidly screen plant-derived compounds for their binding potential against COX-1 and COX-2. MM-GBSA post-docking was performed to provide a more accurate estimation of ligand binding free energy (ΔGbind), incorporating solvation effects, protein flexibility, and detailed energetic contributions, offering a comprehensive evaluation of ligand-protein interactions. Extra Precision (XP) generates more accurate binding poses and detailed interaction profiles. In the docking procedure, the various conformations for the ligand were generated, and the final energy refinement of the ligand pose was performed[61]. For each tested bioactive compound, the docking score of the best pose interacting with the target proteins was calculated[62].

Next generation sequencing

The next-generation sequencing was performed by Inqaba Biotec Industries (South Africa). The RNA fragments were analyzed on a bioanalyzer. The sequencing library was prepared using the MiSeq RNA-0 rRNA reduction library kit from Illumina. Sequencing was performed on a NextSeq550 system[63]. Paired-end sequencing was carried out at a depth of 10 million bases for 300 cycles. Following sequencing, the raw sequencing data was analyzed using the Galaxy platform (Galaxy Europe) (galaxyproject.eu) with a pipeline consisting of the following tools: Trimmomatic was used to trim the reads, and FastQC was used to generate the quality control reports[64]. HiSAT2 was used to align the read. Differential gene expression was then analyzed using the Limma package (limma-voom). The HG38 human genome was used as the reference genome, and reference mapping was performed using Bowtie 2. Volcano plots were created using GraphPad Prism, and PANTHER was used to perform gene ontogeny analysis[65]. Pathway analysis was performed using PANTHER, Ingenuity Pathway Analysis, and Reactome[66]. Finally, the transcript levels of genes involved in apoptosis and the cell cycle were obtained from the data and plotted in order to identify apoptosis- and cell cycle-related genes whose transcription levels were altered by treatment with the water-soluble extract.

Statistical analysis

In our project, a one-way ANOVA was performed followed by Tukey's test for pairwise mean comparison to analyze the data obtained from apoptosis and cell cycle assays. This statistical approach is crucial for identifying significant differences among multiple treatment groups, particularly in studies examining the role of COX-2 in apoptosis. The application of one-way ANOVA is well-established in the analysis of variance among different treatment groups, allowing researchers to determine if there are statistically significant differences in the means of the groups being compared[67–69].

Results

The cytotoxic effects of *T. violacea* leaf extract on normal and TNBC cancer cell l lines

The IC_{50} values were determined using both real-time cell analysis and the reduction of Alamar Blue. The xCELLigence system can produce time dependent physiological IC_{50} values, which can be more revealing than single EC_{50} endpoints used in traditional toxicity testing. Figure 2A shows the growth curve for MDA-MB231 (parental breast adenocarcinoma cell line, TNBC cell line) cells treated with various concentrations of both the water and methanol-soluble *T*, *violacea* extracts, and the positive control (25μM 5-fluorouracil (5FU)), as well as a growth control containing media alone and another continuing media with DMSO at a final concentration of 0.2%. The intermediate concentration of the water-soluble extract was observed to have similar effects to the positive 5FU control. The highest concentration of the extract completely prevents growth and proliferation after a small initial increase. It then appears to kill the cells rapidly. This information was used to plot the logarithmic concentration function (Fig. 2B). This was used to determine the IC_{50} value for the *T. violacea* water-soluble extract to be ~ 395 μg/ml against MDA-MN231 cells and 537 μg/mL for the MCF10A cells (Fig. 2B). This means that a greater concentration of the extract is required to inhibit the growth of 50% of the MCF-10 A cells. This indicates that the *T. violacea* extract may exhibit preferential cytotoxicity towards TNBC cells compared to normal breast cells, a desired trait for prospective anticancer treatments.

DMSO is observed to have an initial inhibitory effect on cell growth, however, the cells seem to recover from this. The lowest and intermediate concentrations of the extract have similar effects on the cells both of which are much lower than the effect observed from treatment with 5FU. The highest concentration of extract decreased growth and proliferation of the cells but only appeared to have cytotoxic effects 40 h after treatment. This information was used to plot the logarithmic concentration function (Fig. 2A). This was used to determine the IC_{50} value for the *T. violacea* methanol soluble extract to be ~ 687 μg/mL (Fig. 2B).

Dimethyl sulfoxide (DMSO) was employed as a multifunctional solvent as described in[70]. In this study DMSO was used to dissolve non-polar compounds extracted using methanol extraction. Although DMSO has positive uses, there have been reports of significant toxicity towards human cell lines[71,72]. Research has pointed out the possible dangers of DMSO, such as its toxicity and negative impact on human health[70]. Concerns of neurotoxicity linked to DMSO have been highlighted in the cryopreservation of hematopoietic cells[73]. Research has investigated the disintegration of DMSO, uncovering the creation of several decomposition products under particular circumstances[74]. Research has been conducted on the autocatalytic breakdown of DMSO because of safety issues associated with its usage as a solvent[71,74]. Research has also examined the heat degradation of DMSO and its significance in chemical processes[75]. As a result of this in our study DMSO was initially limited to a final concentration of 0,5%. However, this failed to dissolve the powdered methanol soluble extract. As such the DMSO concentration increased until the extract was dissolved. This only occurred at a concentration of 2% DMSO.

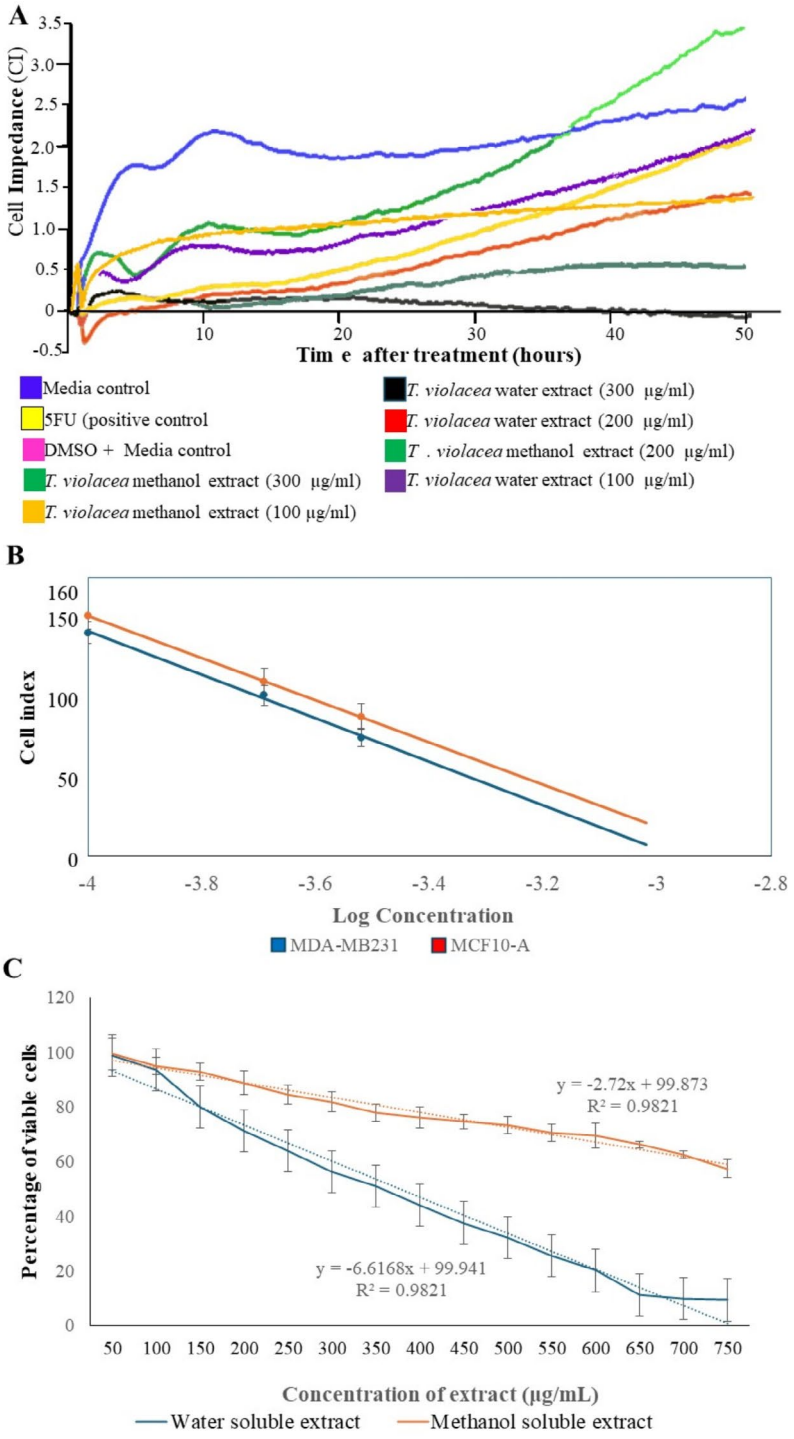

Fig. 2. IC_{50} determination for the *T. violacea* water and methanol-soluble extract on MDA MB231 TNBC cells (A and B) using RTCA analysis. (**A**) The growth curves for both extracts at various concentrations, including a media-only and a medium-vehicle control as well as a positive control, which consisted of 5FU at a sub-lethal level. (**B**) Determination of the IC_{50} by the RTCA software based on CI being plotted as a function of cell viability using the controls and the log of the extract concentration. This method gave IC_{50} values of 395 µg/mL for the MDA-MB231 cells and 537 µg/mL for the MCF-10 A cells (**C**) Determination of the IC_{50} value for the extracts using Alamar Blue assays. These assays indicated that the water-soluble extract had much higher activity than the methanol-soluble extract. Despite this, the RTCA and Alamar Blue assays gave similar results for both the water-soluble extract (395 and 359 µg/mL) and the methanol-soluble extract (820 and 863 µg/mL). All experiments were performed with three technical replicates of three biological replicates. A sample of the data from the RTCA assay is given in Appendix 1 Table S1. A sample of the Alamar Blue assay data is given in Appendix 1 Table S2.

In order to perform the Alamar Blue cytotoxicity assay, the cells were treated with various concentrations of extract before being exposed to Alamar Blue for two hours. Living cells are able to reduce the dye through metabolic reactions, leading to changes in the color and fluorescence of the dye. These changes can be measured on a plate reader, and the percentage of viable cells can be calculated by comparing them to an untreated control. In Fig. 2C, it can be seen that the IC_{50} value for the *T. violacea* water-soluble extract was 350 µg/mL, with the linear relationship between concentration and viability represented by an R squared value of 0/9572. The activity of this *T. violacea* water extract isolated from leaves showed the strongest cytotoxicity against the TNBC cancer cell lines. Much stronger than the activity observed for the *T. violacea* methanol-soluble extract represented in Fig. 2C (820 µg/mL). This extract still demonstrated a linear relationship between concentration and viability, implying that despite its poor activity, it still had a concentration-dependent effect on cell viability. *T. violacea* water-soluble extract and *T. violacea* methanol-soluble extract have similar IC_{50} values in the Resazurin/Alamar Blue cell viability assays and the xCELLigence real-time cell analysis (RTCA) system. Due to the high IC_{50} values determined for the methanol-soluble extract and the difficulties associated with dissolving this extract in a non-lethal concentration of DMSO, the majority of further experiments focused solely on the *T. violacea* water-soluble extract.

Pro-apoptotic and anti-proliferative activities of T.violacea water soluble extracts

As a consequence of the anticancer activity observed in the cytotoxicity assays, further investigations were made into the possible pro-apoptotic activity of these plant extracts. An apoptosis detection assay was performed to determine if the anti-proliferative impact of *T. violacea* crude extracts was caused by apoptosis or necrosis. Cells were treated with *T. violacea* crude extracts for 75 h with a concentration lower than the IC_{50}, the IC_{50} concentration, and a concentration higher than the IC_{50} before being stained with Annexin-V/propidium iodide (PI) dyes to identify living cells from apoptotic and necrotic cells. Because of their potential to die via necrosis, heat-killed cells were included as a positive control.

The positive control cells were used to calibrate the Luminex Guava Muse® cell analyzer, as most of the cells could be gated as dead cells (Fig. 3A, B). The untreated control for both cell lines showed most of the cells gathered in the live quadrant, with 86.5% alive for the MCF10A (normal breast epithelial cell line) cells (Fig. 3A) and 79.2% for the MDA-MB 231 cells (Fig. 3B). Here, less than 10% of either cell line stained for signs of apoptosis, and only 4.75% of the MCF10A cells were dead. A much larger percentage of the MDA-MB 231 cells (19%) were dead, but the majority of the cells were alive. Following treatment, the vast majority of the MDA-MB-231 cells were dead or dying, with 82% in the late stages of apoptosis (Fig. 3B). In contrast to this, while the extract did induce apoptosis in the MCF10A cells, over 58% of these cells were still alive 72 h after treatment (Fig. 3A), compared to only 4.7% of the MDA-MB231 cells. The therapy induced greater levels of apoptosis in the TNBC cell line compared to normal breast cells. IC_{50} values are determined by nonlinear regression analysis to properly predict the IC_{50} value by fitting the dose-response curve.

Further experiments using various concentrations of this extract revealed that this increase in the apoptosis levels in the TNBC cells was concentration-dependent, with concentrations half that of the IC_{50} causing little to no apoptosis. Here, the number of viable cells was similar to that of the untreated cells (Fig. 3C). Interestingly, treatment did result in a higher number of cells dying due to necrosis, while most of the untreated cells died due to apoptosis. Treatment with concentrations at or higher than the IC_{50} led to higher levels of apoptosis and a massive decrease in cell viability. Treatment of the normal MCF10A breast cells clearly led to a significant increase in cell death. However, this was to a lesser extent than the apoptotic effects observed in the TNBC cells treated with the same concentration of water-soluble extract.

In order to determine the effects of active plant extracts on the ability of treated cells to progress through the cell cycle, the DNA content was determined using flow cytometry and propidium iodide (PI) staining. The cells were treated as before with three different concentrations of *Tulbaghia violacea* water-soluble extract. One concentration below the IC_{50}, one above the IC_{50} for 48 h. Figure 4 depicts the results of the cell cycle assay performed on the TNBC and normal cell lines. The higher concentration was also used to treat the normal breast cells. The results show that in either the TNBC or normal breast cells, treatment of the cells led to an increase in the number of cells in the s phase. Cell cycle analysis (Fig. 4) indicated that treatment with the water-soluble extract of *Tulbaghia violacea* resulted in a reduction in the proportion of TNBC cells in the G0/G1 phase. This trend was consistent across concentrations and in both TNBC and normal breast cancer cell lines. This may be due to the activation of the intra-S-phase checkpoint and a decrease in the number of cells in the G0/G1 phase. This checkpoint is known to be activated in response to stalled replication forks following DNA damage[76]. It is possible that a component of the crude water-soluble extract is able to inhibit to stall replication leading to the S phase checkpoint arrest. This observed increase in the S-phase does not conclusively support the activation of an S-phase checkpoint. The observed shift in cell populations could be due to alterations in cell cycle progression rather than true checkpoint activation. The extent of the shift toward the S-phase was modest. As such the extract may not robustly stall cells in the S-phase but could instead influence the balance of progression between G0/G1 and S-phase. This effect could be attributed to potential cytotoxic stress.

Determining the composition of the extract

Figure 5 shows the NMR spectrum obtained from the analysis of the water-soluble *T. violacea* extract. This analysis identified approximately 51 separate compounds. These compounds seemed to be more easily identified by the NMR analysis. A list of some of the compounds studied by these analyses is given in Table 1. The number of each class of compound is depicted in Fig. 6.

These compounds were detected and quantified, presenting a variety of structures and molecular weights. The specific biological activities and potential therapeutic applications of these compounds have been noted, and they range from anti-cancer activity to apoptosis induction and other biological activities. The detailed

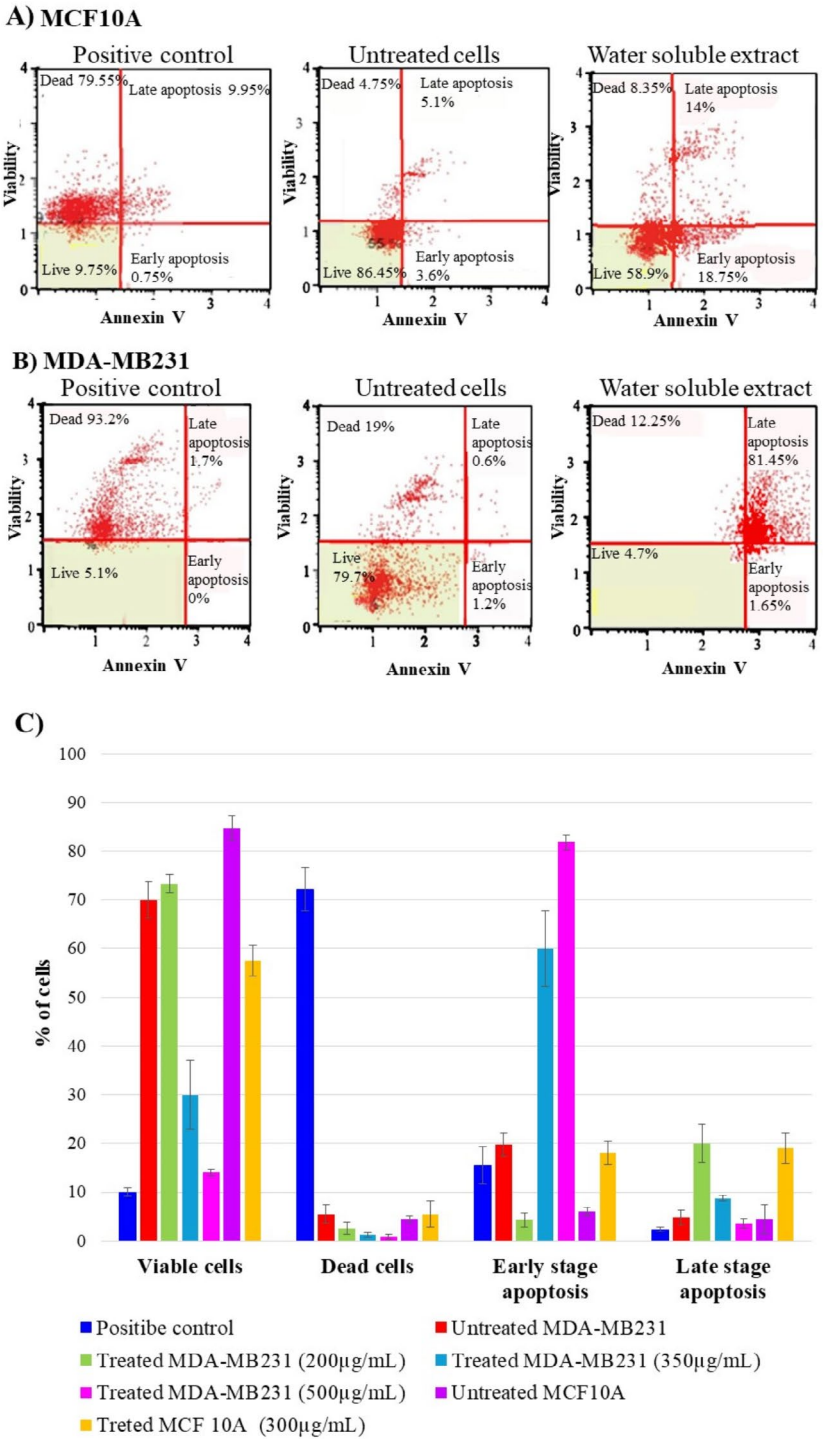

Fig. 3. Apoptosis (Annexin V Assay). The figure displays the findings of an Annexin V experiment comparing apoptosis in two cell lines: MCF10A (normal breast cells) and MDA-MB231 (triple-negative breast cancer cells). Panel A shows the MCF10A cell line under three conditions: a positive control with high late apoptosis/dead cells, untreated cells mostly containing living cells, and cells treated with a water-soluble extract displaying higher early apoptosis. Panel B displays the MDA-MB231 cell line under three identical settings, where treatment with the water-soluble extract led to a notable rise in both early and late apoptosis. Panel C displays a bar graph showing the proportion of viable, dead, early-stage apoptotic, and late-stage apoptotic cells under various treatments and concentrations for both cell lines. The flow cytometry gating approach was standardized by employing heat-killed cells to establish the dead cell quadrant, guaranteeing uniform analysis among samples. Cells were categorized according to their staining with Annexin V and a dead cell stain. Viable cells were negative for both stains, early-stage apoptotic cells were positive for Annexin V alone, and late-stage apoptotic or dead cells were positive for both stains. The graph displays p-values above the bars.

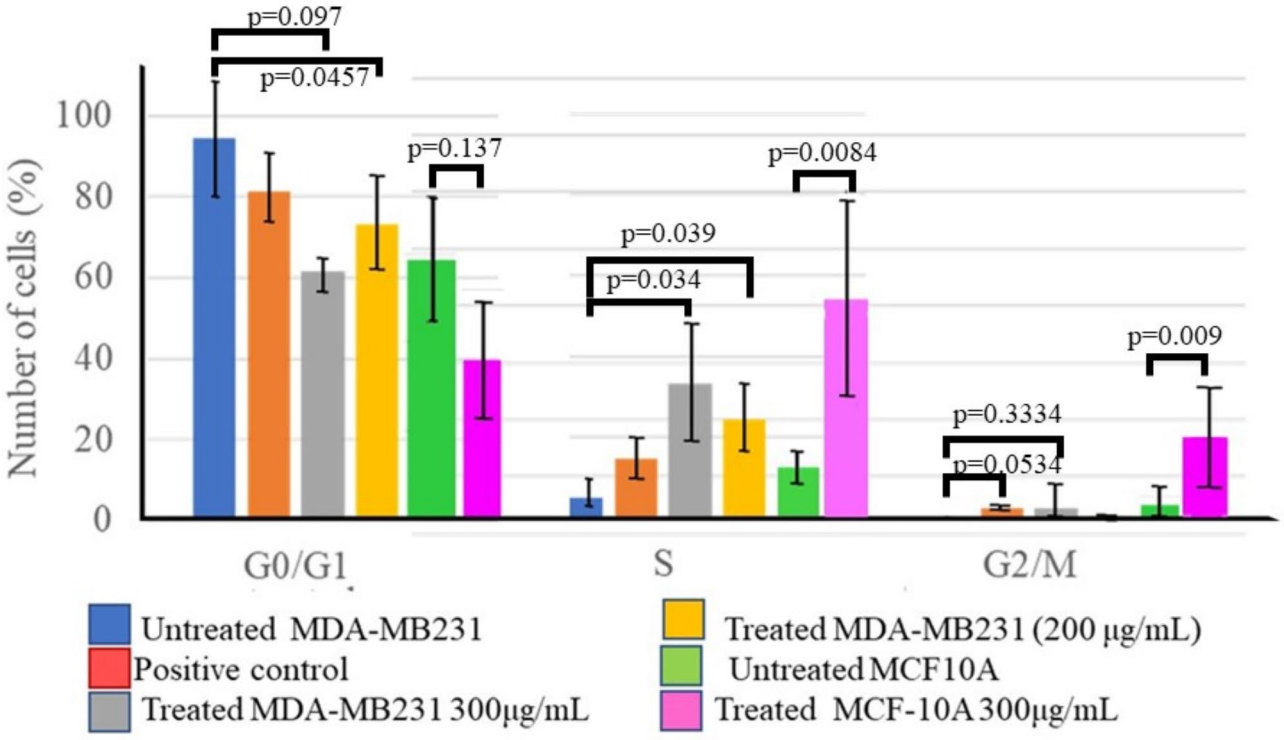

Fig. 4. Cell cycle assay. The Cell cycle analysis indicated that treatment resulted in a reduction in the proportion of TNBC cells in the G0/G1 phase. This trend was observed in both TNBC and normal breast cancer cell lines. The observed increase in the S-phase does not conclusively support the activation of an S-phase checkpoint. The observed shift in cell populations could be due to alterations in cell cycle progression rather than true checkpoint activation. The extent of the shift toward the S-phase was modest. As such the extract may not robustly stall cells in the S-phase but could instead influence the balance of progression between G0/G1 and S-phase. This effect could be attributed to potential cytotoxic stress.

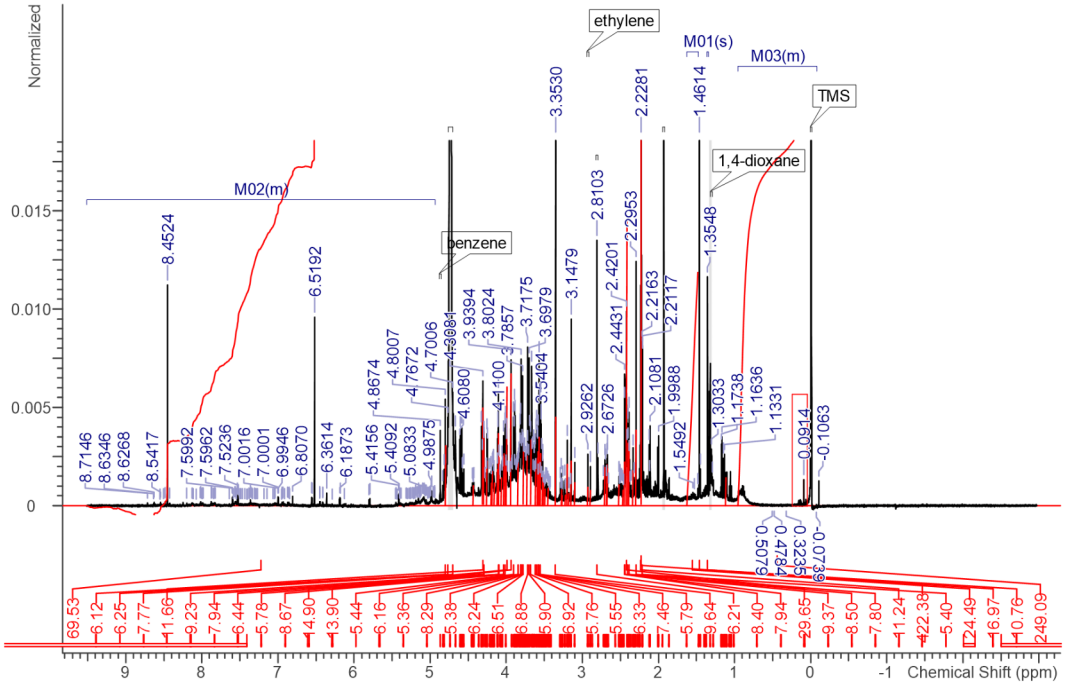

Fig. 5. Determination of the molecular composition of the *T. violacea* water-soluble extract. The figure represents an NMR spectrum of *T. violacea* water-soluble extract.

Phytochemical compound	Exact mass	Formula	Refs
Anti-cancer			
4 H-Pyran-4-one, 2,3-dihydro-3,5-dihydroxy-6-methyl-(DDMP)	144.12	C6H8O4	86–89
1,2,4-Triazine-3,5(2 H,4 H)-dione	113.08	C3H3N3O2	90–92
d-Glycero-d-galacto-heptose	210.18	C7H14O7	93
Benzaldehyde, 4-(1-methylethyl)	148.20	C10H12O	94
Vanillin	152.15	C8H8O3	95
Oxime-, methoxy-phenyl	151.16	C8H9NO2	96
Pyrrolidine	71.12	C4H9N	97
Schizandrin	432.5	C24H32O7	98,99
Taurolidine	284.4	C7H16N4O4S2	
alpha.-Pinene	136.23	C10H16	
Neurotransmitter inhibitors			
Terbutaline, N-trifluoroacetyl-o, o,o-tris(trimethylsilyl)deriv.	537.8	C23H42F3NO4Si3	100–102
Benserazide	257.24	C10H15N3O5	103–105
Antidiarrheal			
Difenoxin	424.5	C28H28N2O2	106
Anticonvulsant			
Mephobarbital	246.26	C13H14N2O3	107
Analgesic, anti-inflammatory			
Antipyrine	188.23	C11H12N2O	108–110
Antibiologicals (antibiotic. antivirals, antiseptics and antifungals)			
Tricyclo [3.3.1.1(3,7)] decan-1-amine	151.25	C10H17N	111,112
Thymol	150.22	C10H14O	113
Benzenepropanoic acid	150.17	C9H10O2	114–118
Cycloserine	102.09	C3H6N2O2	119,120
2-Propen-1-amine	57.09	C3H7N	121–125
Vasodilator			
Cyclandelate	276.4	C17H24O3	126–134
Sedative			
Ethchlorvynol	144.60	C7H9ClO	135,136
Anxiolytic and muscle relaxant			
Emylcamate	145.20	C7H15NO2	137,138
Fumigant and larvicide			
Methyl formate	60.05	C2H4O2	139
Marine xenobiotic metabolite			
Cycloheptasiloxane, tetradecamethyl-	519.07	C14H42O7Si7	140,141
Highly toxic lachrymator			
Cyanogen chloride	61.47	CNCl	142142.

Table 1. The chemical composition of crude water-soluble *T. violacea* extract.

mechanisms of action and potential therapeutic implications are subjects for further research. The therapeutic potential of these compounds, particularly those with anti-cancer properties, is of significant interest and warrants additional investigation. Previous research has revealed that *T. violacea* contains anticancer chemicals such as flavonoids, polyphenols, and saponins[31,77] see Table 2[31,77]. Flavonoids have the capacity to trigger apoptosis, prevent angiogenesis, and disrupt the cell cycle by breaking down the structure of the spindle fiber[78]. Polyphenols have been shown to inhibit cancer cell proliferation by triggering cell cycle arrest, apoptosis, and cell signaling[79].

The Amaryllidaceae family has over 900 species clustered into 75 genera. The family contains a unique class of specialized metabolites known as Amaryllidaceae alkaloids (AAs). They are made up of heterocyclic nitrogen bridges. Over 650 AAs have been isolated thus far and has the isoquinoline nucleus as the basis for their structure[80]. Amaryllidaceae alkaloids are of main interest because of their cholinesterase inhibition potential[81,82], . In our study we identified various alkaloids although these were not the majority of the compounds isolated. Another member of the family, the perennial herb Hymenocallis littoralis (Amaryllidaceae) contains many non-alkaloid components in the extract. These include compounds such as undulatoside A, 8-methylnaringenin and syzalterin[83]. As well as compounds with a similar structure to each other which have structures similar to many of the compounds we isolated. These include compounds such as 6-methylapigenin, 6-methyl-aromadendrin, 5,7-dihydroxy-6,8-dimethoxy-2-hydroxymethyl-4 H-chromoen-4-one, 4',5,7-trihydroxy-8-methylflavanone, 4',7-hydroxy-8-methylflavanone, isoliquiritigenin, 7,4'-dihydroxyflavane, naringenin and 8-demethylfarrerol[83].

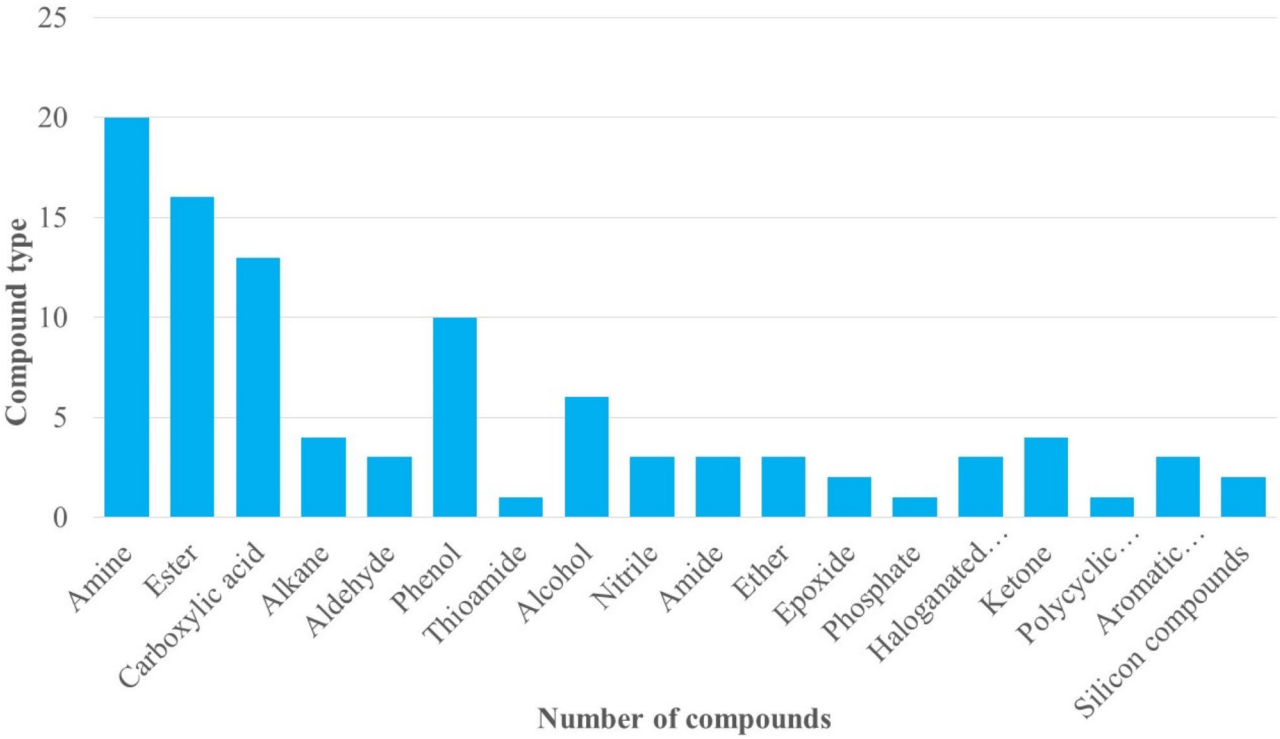

Fig. 6. The number of different types of compounds identified in the *T. violacea* water soluble extract. The majority of the identified compounds are Amines, Esters and carboxylic acids. In addition to these there are a relatively high number of phenols.

Compound name	Molecular pattern	Concentration	References
4 H-Pyran-4-one, 2,3-dihydro-3,5-dihydroxy-6-methyl (DDMP)	A pyran derivative with antioxidant properties	More than 100 ppm from 10 mg/µL biomass extract	143
d-Glycero-d-galacto-heptose	A seven-carbon sugar	Present in biological samples, associated with exopolysaccharide carbohydrate structures and biofilm formation	144,145
1,2,4-Triazine-3,5(2 H,4 H)-dione	A triazine derivative	High ant staphylococcal potential at a concentration equal to 1 µg/mL or lower	146
Benzaldehyde, 4-(1-methylethyl)	An aromatic aldehyde	Not specified	147
Vanillin	A phenolic aldehyde, a primary component of the extract of the vanilla bean	Not specified	148
Schisandrin	A lignan found in the fruits of Schisandra chinensis	Not specified	149,150
Oxime-, methoxy-phenyl	A phenyl oxime derivative	Not specified	151,152
Pyrrolidine	A simple organic compound and a secondary amine, the pyrrolidine core is one of the simplest alkaloid structures	Not specified	153–155
Taurolidine	A derivative of the amino acid taurine	Not specified	156–158
α-pinene	A bicyclic monoterpene	Not specified	159

Table 2. Concentration and molecular characteristics of selected compounds with biological and chemical significance.

Pyrrolidine was one of the compounds isolated and the pyrrolidine ring structure is found in many alkaloids from this family. Another member of the family found in South Africa *Boophone haemanthoides* extract contained various compounds such as distichamine, 1α,3α-diacetylnerbowdine, hippadine, stigmast-4-ene-3,6-dione, cholest-4-en-3-one, tyrosol, and 3-hydroxy-1-(4'-hydroxyphenyl)-1-propanone[84]. The compound tyrosol is a derivative of phenyl alcohol and is found in multiple natural sources. This is similar to taurine which is naturally derived from cysteine, and we isolated a compound with similar characteristics to the taurine derivative taurolidine.

Of particular interest in relation to medicinal compounds are alkaloids which are found in many medicinal plants. These nitrogenous organic compounds and possess pharmacological effects[85]. Alkaloid compounds isolated from *T. violacea* are shown in Table 3. These compounds are nitrogen-containing and could be classified as alkaloids due to their structures and properties.

Chemical name	Chemical formula	Molecular weight (g/mol)
Piperidine	$C_5H_{11}N$	85.15
1-Naphthalenamine	$C_{10}H_9N$	143.19
Piperidine, 1-nitroso-	$C_5H_{10}N_2O$	98.15
Tricyclo[3.3.1.1(3,7)]decan-1-amine	$C_{10}H_{17}N$	151.25

Table 3. Alkaloid like compounds identified in the *T. violacea* water soluble extract.

Computational modelling of the interaction of COX-2 and components of the *T. violacea* water soluble extract

The phytochemical components of the water-soluble crude extract from the leaves of *T. violacea* showed significant activity against the TNBC cell line MDA-MB231, implying that it or its constituents may hold therapeutic promise in the treatment of triple-negative breast cancer. The presence of various bioactive compounds with diverse pharmacological properties was confirmed by NMR analyses. The ability of these bioactive chemicals to induce apoptosis in the TNBC cell line was investigated using in silico molecular docking with COX-2, a known apoptosis inhibitor and COX-1 a promoter of apoptosis.

The binding analysis of COX-1 and COX-2 and ligands revealed that the binding pattern varied depending on the nature of the ligands. A comparison of the two structures for COX-1 and COX-2 revealed a root-mean-square deviation (RMSD) value for the binding site and protein backbone residues of 344.3582 and 367.4478 respectively, revealing that there were significant deviations in the binding site residues and the global backbone structure of the two proteins differs substantially. The SiteMap analysis revealed the most druggable site for COX-1is sitemap_Cox1_site_5, with the highest Dscore (1.333) and SiteScore (1.268), despite its relatively small volume (154.693 $Å^3$). This suggests a highly specific and well-defined binding pocket. For COX-2, sitemap_Cox2_site_2 emerges as the most promising binding site, with a Dscore of 1.077, SiteScore of 1.055, and a substantial volume of 611.569 $Å^3$. This site combines size and druggability, making it an ideal candidate for docking. Despite their structural similarity, COX-1 and COX-2 exhibit notable differences in their binding site properties due to variations in amino acid composition, functional roles, and conformational states.

Figure 7 depicts the docking results of bioactive compounds, while Table 4 shows the docking scores and ΔG values for the docking of these various compounds with the two proteins. Anticancer docked ligands received scores ranging from − 2 to -9.5 for COX-2 and from − 0.7 to -6.2 for COX-1.

The docking scores of the interaction between D-Glycero-d-galacto-heptose and the active site of COX-1 indicate a favourable binding conformation. The binding free energy (MM-GBSA ΔG Bind) was − 13.117 kcal/mol, and the Prime Energy was calculated as -20658.00 kcal/mol, demonstrating strong binding stability. The binding of D-Glycero-d-galacto-heptose within the COX-1 active site was mediated by multiple key residues through specific molecular interactions. Ser530 played a critical role in anchoring the ligand via a hydrogen bond between its hydroxyl side chain and one of the ligand's hydroxyl groups. This interaction stabilized the ligand in the binding pocket and contributed significantly to its binding affinity. Important residues for this interaction are Arg120, Val349, Leu384, Ala527, Tyr355. Tyr385 and Glu524. The ligand's polar functional groups were oriented toward hydrogen-bond donors and acceptors, while its nonpolar regions nestled into hydrophobic pockets. This precise orientation maximized its binding efficiency and stability. The docking scores for the molecular docking study of D-Glycero-d-galacto-heptose within the active site of COX-2 (PDB ID: 5IKT) signified a strong and favorable interaction. D-Glycero-d-galacto-heptose formed key interactions with several residues, Tyr385, Ser530, Val349, Leu384, Arg120, Glu524, Tyr355 and Phe518, which provided a stabilizing nonpolar environment. These residues surrounded the ligands. The simulated interaction of 2,3-dihydro-3,5-dihydroxy-6-methyl-4 H-pyran-4-one (first tautomer), with COX-1 indicated a stable interaction through hydrophobic interactions and additional polar contacts. The first tautomer of 2,3-dihydro-3,5-dihydroxy-6-methyl-4 H-pyran-4-one shows the most favourable binding properties with COX-1. The interaction of ,3-dihydro-3,5-dihydroxy-6-methyl-4 H-pyran-4-one with COX-2 showed an even stronger interaction than that predicted for the interaction with COX-1. Key interactions differ significantly between the two isoforms. COX-1 stabilization is driven by hydrophobic interactions, COX-2 interactions are dominated by hydrogen bonds. Vanillin shows high docking scores with both COX-1 and COX-2, The interaction with COX-1 relies on strong hydrogen bonding. The secondary tautomer of vanillin demonstrated a weaker binding. The interaction of COX-2 with Vanillin shows close to the same binding energies to those of COX-1. COX-2 shows an interaction with vanillin that relies on a single strong hydrogen bond is observed between THR206 and the hydroxyl group of vanillin, further stabilizing its placement within the active site.

The molecular docking study of 1,2,4-Triazine-3,5(2 H,4 H)-dione and its primary tautomer with COX-2, suggested the binding site has an ideal environment for ligand accommodation. These data highlight the compound's capacity for stable and specific interaction with COX-2. The docking analysis of Benzaldehyde,4-(1-methylethyl) with the COX-1 enzyme. This interaction is primarily stabilized by hydrophobic interactions, with important interacting residues creating a nonpolar environment that complements the hydrophobic regions of the ligand. The docking analysis of Oxime-, methoxy-phenyl- with the COX-1 demonstrated a favourable interaction with a stable. The interacting residues create a hydrophobic environment that stabilizes the ligand's placement within the active site. Alpha-Pinene exhibits notable interactions within the COX-1 binding site (sitemap_Cox1_site_5) with moderate binding affinity.

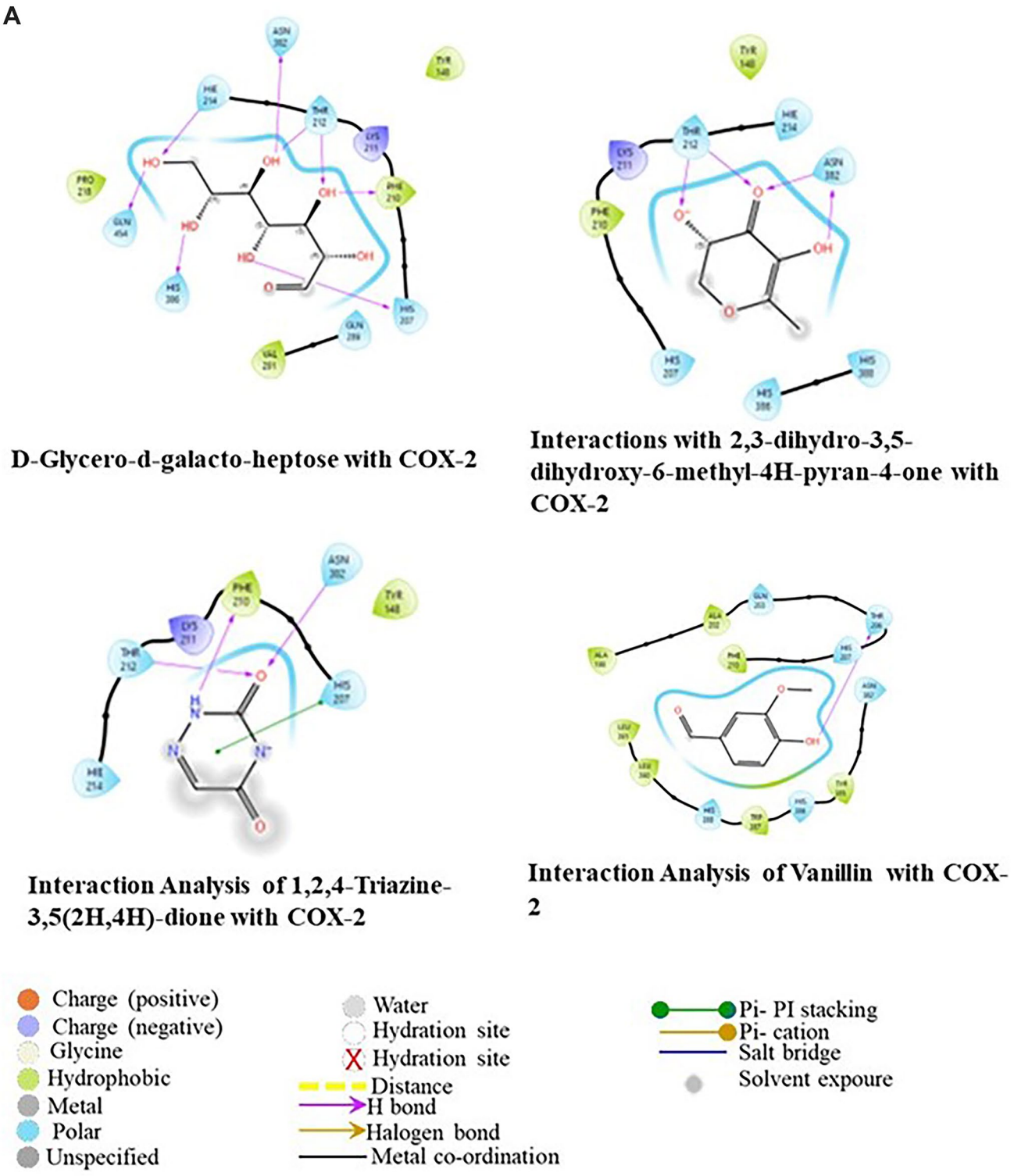

Fig. 7. Molecular docking site for *T. violacea* crude extract compounds with (**A**) COX-2 and (**B**) COX-1 protein. This figure shows the interactions between the structures of specific compounds within the extract and the active and docking sites within the COX-2 protein (viewed using Schrodinger software).

Establishing the transcription levels of genes associated with apoptosis and the cell cycle following treatment of TNBC and normal breast cells

Next-generation sequencing was used to identify genes whose transcription is altered following treatment of the normal breast and TNBC cell lines. Following sequencing, a PANTHER analysis was used to identify genes that play a role in specific molecular and biological functions. We took the genes that play a role in apoptosis

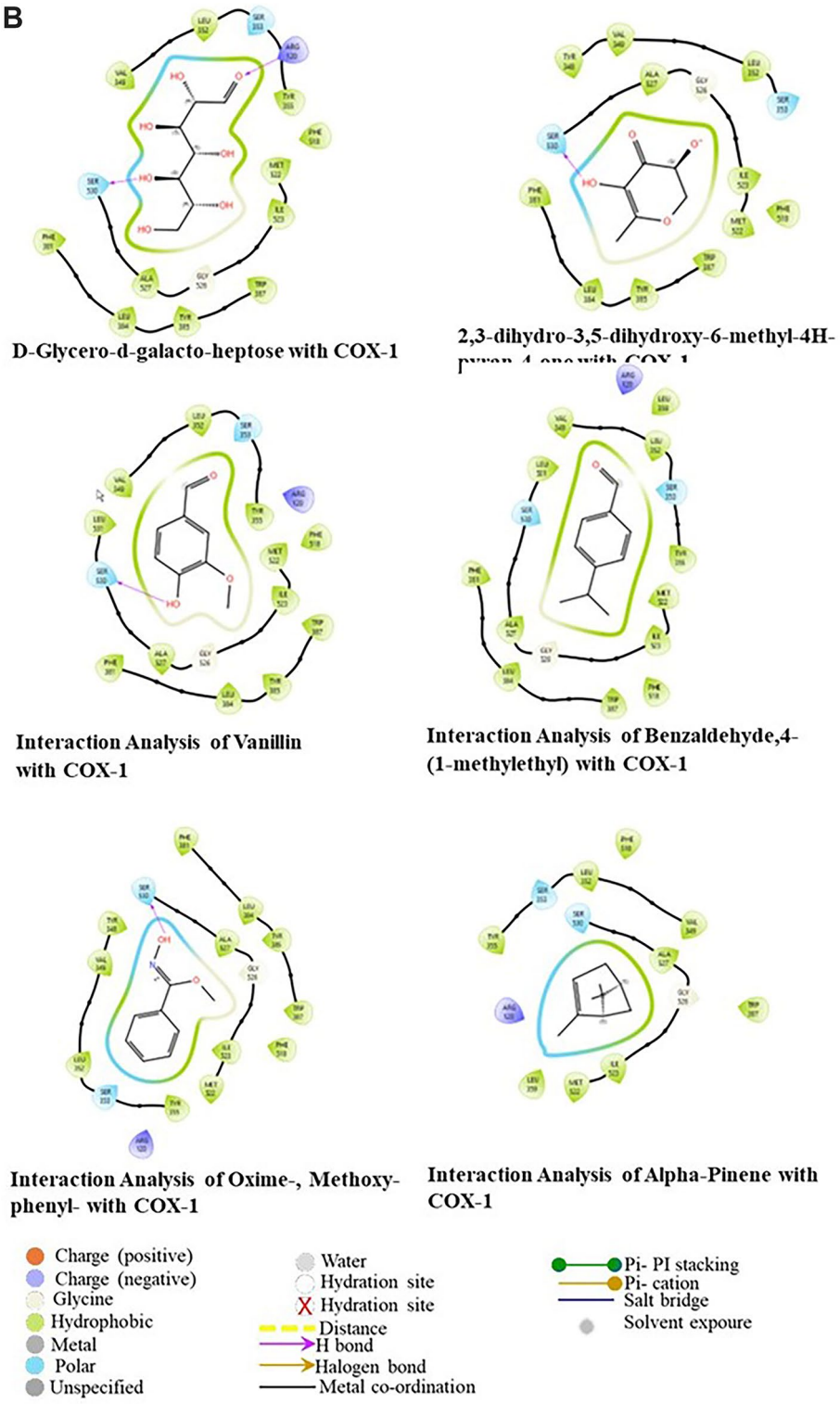

Figure 7. (continued)

and cell cycle control and compared the transcript levels of these genes. Both normal and TNBC cells show an enrichment in the expression of genes involved in apoptosis. The apoptosis assay established that the extract is able to induce apoptosis in both TNBC cells and normal breast cells, although to a lesser extent. By comparing the fold changes in the transcript level of pro- and anti-apoptotic genes as determined by NGS in both pro- and anti-apoptotic genes in both cell lines before and after treatment, we can see if the transcriptome changes reflect the increase in apoptosis following treatment as well as identify the pathways involved. In Fig. 8A, it can be seen that the majority of the pro-apoptotic genes are increased in the TNBC cells following treatment with the extract.

COX-1				
Title	Docking score	XP GScore	MMGBSA dG Bind	Prime Energy
D-Glycero-d-galacto-heptose	-6.7651	-6.7651	-13.1170	-20658.0028
Benzaldehyde,4-(-1-methylethyl)	-6.3468	-6.3468	-29.1853	-20726.7183
Oxime-, methoxy-phenyl-	-5.5491	-5.5519	-30.9127	-20693.0100
Vanillin	-5.3235	-5.5468	-29.0731	-20718.4894
Alpha-Pinene	-5.2502	-5.2502	-12.9280	-20703.2094
2,3-dihydro-3,5-dihydroxy-6-methyl-4 H-pyran-4-one	-5.1472	-5.4743	-19.7579	-20694.3562
2,3-dihydro-3,5-dihydroxy-6-methyl-4 H-pyran-4-one	-5.0830	-5.8820	-25.5945	-20702.2085
Vanillin	-4.0959	-4.7822	27.8365	-20686.8357
2,3-dihydro-3,5-dihydroxy-6-methyl-4 H-pyran-4-one	-3.6277	-4.6971	-8.6822	-20670.9029
1,2,4-Triazine-3,5(2 H,4 H)-dione	-3.1978	-3.2562	28.3651	-20690.4987
Taurolidine	-2.5447	-3.0293	17.9786	-20804.7507
Pyrrolidine	-2.4278	-2.4278	-20.8539	-20707.6149
1,2,4-Triazine-3,5(2 H,4 H)-dione	-1.9008	-3.3750	-21.0430	-20749.7518
6Y3C - prepared_ligand3	-1.0801	-1.0817	60.1087	-20717.8525
6Y3C - prepared_ligand2	-1.0801	-1.0817	60.1087	-20717.8525
6Y3C - prepared_ligand1	-1.0801	-1.0817	60.1087	-20717.8525
1,2,4-Triazine-3,5(2 H,4 H)-dione	-0.4109	-3.0962	18.8640	-20761.0050
Taurolidine	-0.2968	-0.7763	23.1361	-20772.5793
Taurolidine	0.7226	-0.5667	33.7933	-20760.7993
COX-2				
Compound	Docking score	XP GScore	MMGBSA dG Bind	Prime energy
D-Glycero-d-galacto-heptose	-9.5225	-9.5226	-44.7095	-22109.9911
5IKT - prepared_ligand1	-6.1895	-6.1900	-19.1736	-22165.1467
2,3-dihydro-3,5-dihydroxy-6-methyl-4 H-pyran-4-one	-6.0627	-6.3898	-18.1056	-22119.8241
1,2,4-Triazine-3,5(2 H,4 H)-dione	-5.9708	-6.0292	-7.3101	-22150.5119
Vanillin	-5.2671	-5.4904	-33.1467	-22146.4313
Benzaldehyde,4-(-1-methylethyl)	-4.9004	-4.9004	-22.9260	-22144.4999
Oxime-, methoxy-phenyl-	-4.8821	-4.8849	-23.9147	-22112.2325
Taurolidine	-4.8802	-5.3648	-13.9191	-22260.7056
2,3-dihydro-3,5-dihydroxy-6-methyl-4 H-pyran-4-one	-4.6671	-5.7365	-22.1185	-22110.4496
1,2,4-Triazine-3,5(2 H,4 H)-dione	-4.6347	-6.1089	-27.1404	-22180.0280
2,3-dihydro-3,5-dihydroxy-6-methyl-4 H-pyran-4-one	-4.4544	-5.2534	-25.4832	-22121.2281
Alpha-Pinene	-3.7537	-3.7537	3.7171	-22110.6590
Taurolidine	-3.6975	-4.1770	-14.3457	-22232.32664
Vanillin	-3.4091	-4.0954	6.0500	-22132.4437
1,2,4-Triazine-3,5(2 H,4 H)-dione	-3.0127	-5.6980	-15.6523	-22219.4573
Pyrrolidine	-2.6101	-2.6101	-21.7251	-22132.5875
Taurolidine	-2.5258	-3.8150	-12.0192	-22230.9520

Table 4. Molecular docking score for the anticancer bioactive compounds of *T. Violacea* water crude extract with the COX-1 and COX-2 proteins.

It also appears that both the extrinsic and intrinsic apoptotic pathways are upregulated (Fig. 8A,B). The cell cycle experiment confirmed that the extract had an effect on the cell cycle of these cells, particularly on the S phase of the cell cycle, resulting in an increased number of cells in the S phase in both TNBC cells and normal breast cells. We examined the fold changes in gene transcript levels associated with S phase advancement and arrest by examining NGS data from both cell lines before and after treatment. This analysis aimed to establish if the observed transcriptome alterations align with the S phase arrest seen post-treatment (Fig. 8C,D).

The difference in the number of genes examined in normal and cancer cells seen in Fig. 8 is due to a focused strategy that targets genes linked to cancer cell behavior and carcinogenesis[160]. This focused strategy is based on the understanding that cancer cells display unique gene expression patterns that play a key role in the progression of the disease[160]. Technical limitations and the requirement to standardize data for cancer occurrence may possibly play a role in this specific analysis[160]. The lack of statistical analysis in the study prevents making conclusive statements on the treatment's effect on gene expression, highlighting the need for strong analytical procedures in similar research[160].

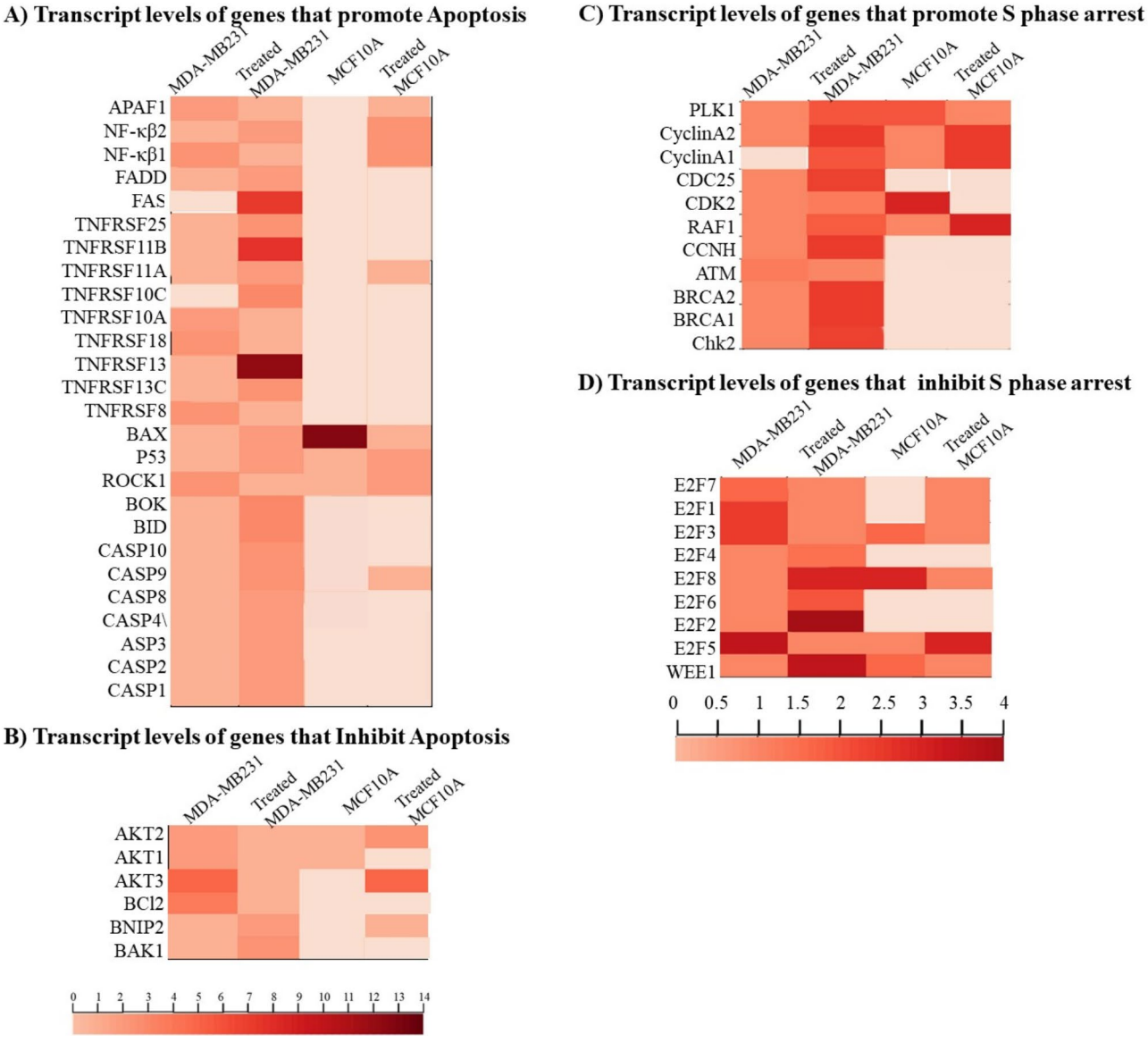

Fig. 8. The mRNA levels of apoptosis-related and Cell cycle genes as determined by NGS before and after treatment with the *T. violacea* water-soluble extract. (**A**) Shows the fold change in expression of pro-apoptotic s before and after treatment. (**B**) Shows the fold change in the transcript level of anti-apoptotic genes before and after treatment. (**C**) Shows the fold change in transcripts of genes that promote a stall in the cell cycle at the S phase before and after treatment (**D**) Shows the fold change in transcript level of genes that promote S phase progression before and after treatment. The difference in the number of genes listed for normal and TNBC cells in Fig. 8 reflects a focused strategy that prioritizes genes associated with cancer-specific pathways and behaviour. This selection is based on established evidence of their role in carcinogenesis. Technical limitations and normalization during NGS analysis may also contribute to this discrepancy. The bar chart accurately represents the selected genes for each condition, aligned with the study's objectives."

Discussion

In previous studies, extracts from the leaves of *T. violacea* and not from the bulbs were found to induce apoptosis in cultured cell lines generated from human cancer tissue[30,161]. This triggering of apoptosis was thought to be connected with the activation of caspase-3 and the generation of reactive oxygen species (ROS)[32,162–164]. In our study, water-soluble extracts from the leaves of *T. violacea* were shown to have cytotoxic activity against the TNBC cell line, MDA-MB-231. The methanol-soluble extract was shown to have much lower cytotoxic activity than its water-soluble counterpart. The cytotoxicity values were determined using the RTCA xCELLigence system and an Alamar Blue cytotoxicity assay. Although the precise amounts obtained from the two procedures differed, they exhibited consistent patterns, indicating that the *T. violacea* water-soluble extract was the more cytotoxic. Due to the exact nature of the RTCA method, it could be said that these results were preferable and could be adopted as the true IC_{50} value. The low cytotoxic activity determined for the methanol-soluble extract

may also be due to the poor solubility of the extracted powder. The inconsistent nature of this extract and the large IC_{50} value led to its exclusion from future experiments, including both the apoptosis and cell cycle assays.

An annexin-V death detection assay indicated that the extract induced apoptosis in MDA-MB-231 cells, whereas non-cancerous MCF10A cells were less sensitive, with apoptosis being induced but to a lesser extent. Furthermore, the *T. violacea* water extract induced apoptosis. in a dose- and time-dependent manner. This implies that the cell death resulting from treatment of MDA-MB231 cells with this extract is due to the induction of apoptosis signaling pathways and that these apoptotic genes or pathways are not induced to the same extent in the MCF-10 A cell line. This implies that the extract is specifically targeting molecular differences in the TNBC cells to induce apoptosis. The rate of apoptosis has a substantial impact on the lifetime of both normal and malignant cells[165–168]. The extract was able to trigger apoptosis in such a way that 72 h after treatment, the majority of cells were in late-stage apoptosis, from which they could not recover. Although the half-life of the crude extract in cell culture conditions was not experimentally determined, it appears that the compound's activity was predominantly observed within the first few hours post-treatment. Notably, there was no observed recovery even 72 h later.

The ability of DNA damage to trigger cell-cycle checkpoints and the role of cell cycle progression in carcinogenesis means that much information regarding the mode of action of the extract can be inferred from its effect on the cell cycle progression of cells following treatment[169–172]. Triple-negative breast cancer (TNBC) cells have unique features in their cell cycle dynamics as compared to untreated normal breast cells. Untreated TNBC cells are mostly in the G0/G1 phase, suggesting a condition of dormancy or quiescence[173,174]. TNBC cells exhibit a drop in the G0/G1 phase population and an increase in the S phase when treated with a water-soluble extract, indicating possible DNA damage or replication stress. This change in cell cycle distribution might trigger an S-phase checkpoint that is essential for guaranteeing precise DNA replication[175]. Untreated normal breast cells, (MCF10A cells), have a smaller proportion in the G0/G1 phase compared to TNBC cells, suggesting differences in cell cycle dynamics[176,177]. The water-soluble extract had a comparable effect on both MCF10a and TNBC cells, causing an increase in cells in the S phase. This extract may activate defensive mechanisms for DNA repair and cell viability[178–181]. The extract's effect on metabolite levels and cell behavior highlights the complex interaction between the extract and cellular processes[182,183].

While the data showed a redistribution of cells, with a larger proportion in the S-phase, this alone does not conclusively support the activation of an S-phase checkpoint. S-phase checkpoint activation typically involves specific molecular signals such as DNA damage responses mediated by ATR/Chk1 or replication stress markers such as γ-H2AX. These were not evaluated in the present study, and without such data, the observed shift in cell populations could be due to alterations in cell cycle progression rather than true checkpoint activation. It is also worth noting that although a shift toward the S-phase was observed, the extent of this shift was modest. This suggests that the extract may not robustly stall cells in the S-phase but could instead influence the balance of progression between G0/G1 and S-phase. This effect could be attributed to potential cytotoxic stress, resulting in incomplete progression through the G1 checkpoint or a delay in DNA replication due to partial inhibition of essential factors for S-phase entry. To further validate the hypothesis of S-phase checkpoint activation, additional experiments assessing markers of replication stress or DNA damage, such as phosphorylated Chk1, Chk2, and γ-H2AX, are critical. These experiments would provide mechanistic insights into whether extract-induced effects are related to checkpoint activation or the generalized disruption of cell cycle dynamics.

Natural products have been found to inhibit TNBC cell growth, highlighting the need to comprehend DNA repair mechanisms for successful therapeutic approaches[184,185]. Research has shown that drugs such as simvastatin, obatoclax, and selenite have the ability to halt the proliferation of cancer cells in the G0/G1 phase, emphasizing the complex relationship between cell cycle control and cancer treatment[186–190]. Studying the basic processes that cause these alterations might provide important information for creating new cancer therapies. The water-soluble extract of *T. violacea* has shown the capacity to control DNA replication and metabolite levels in TNBC and normal breast cells, suggesting a complicated interaction that requires more research. It is essential for researchers to comprehend these mechanisms in order to enhance treatment strategies for TNBC patients by utilizing the intricate concepts of cell cycle regulation and DNA repair pathways. The cell cycle dynamics of TNBC cells, the impact of natural products on cell proliferation, and the complicated interplay between DNA repair mechanisms and treatment results highlight the intricate nature of TNBC biology. Additional study in these fields is crucial for progressing our comprehension of TNBC pathogenesis and creating more efficient therapeutic approaches.

Many genes involved in cell cycle control are also involved in apoptosis regulation (for example, *c-myc*, *c-fos*, *p53*, and many kinases and phosphatases)[191–195]. Cell cycle detection based on measuring the DNA content in the cells showed that following treatment of both the normal breast cells and the TNBC cells with the water-soluble *T. violacea* extract, the cells underwent an S-phase checkpoint, accompanied by a decrease in the number of cells in the G0/G1 phase. The majority of the untreated normal and TNBC cells were in the G0/G1 phase. The cell cycle is controlled in a systematic fashion by certain CDKs[196,197]. The S-phase replication checkpoint occurs in response to the stalling of DNA replication forks. This can occur due to lesions or replication perturbations, with the aim of ensuring proper chromosome replication[198–201198]. In mammalian cells, the checkpoint is controlled by ATR[171] and Chk2[202]. The expression of these two kinases is lower in cancer cells[203,204]. The stalling of replication forks in response to single-strand DNA occurs via the activity of the mini-chromosome maintenance complex helicase, which continues to unwind DNA even if replication has stalled[205,206]. The resulting single-strand DNA led to the binding of replication protein A and triggered the activation of the S-phase kinases[198,207,208].

One of the compounds identified was H-Pyran-4-one, 2,3-dihydro-3,5-dihydroxy-6-methyl (DDMP). DDMP has been shown to have DNA strand-breaking activity and mutagenicity[209], which can be detrimental to health. Positive functions of DDMP include the inhibition of colon cancer cell growth by inducing apoptotic cell death via NF-kB inhibition[86,210,211]. Different DDMP concentrations (0.5–1.5 mg/mL) inhibited the growth of

colon cancer cells (SW620 and HCT116), followed by the induction of apoptosis in a dose-dependent manner[212]. H-Pyran-4-one, specifically the derivative 2,3-dihydro-3,5-dihydroxy-6-methyl, has been shown to modulate NF-kB transcriptional activity and DNA binding. This compound is part of a broader class of pyran derivatives that exhibit significant biological activities, including anti-inflammatory and anticancer properties, which are often mediated through the NF-kB signaling pathway[213–215]. The modulation of NF-kB by such compounds can lead to alterations in gene expression that are crucial for cellular responses to stress and inflammation[214,216]. Research indicates that the hydroxyl groups in the 2,3-dihydro-3,5-dihydroxy-6-methyl-4 H-pyran-4-one structure may enhance its interaction with transcription factors, thereby influencing their binding affinity to DNA[217,218]. Moreover, the synthesis of these compounds often involves methods that promote their stability and bioactivity, making them promising candidates for therapeutic applications[219,220]. Furthermore, DDMP inhibited the expression of NF-kB target anti-apoptotic genes (Bcl-2) while increasing the expression of apoptotic genes (Bax, cleaved caspase-3, and cleaved PARP)[86,221–223]. Recent evidence suggests that NF-kB activation is linked to various aspects of oncogenesis, including the regulation of apoptosis, proliferation, differentiation, and cell migration. NF-kB plays a crucial role in promoting cell survival and proliferation, particularly in cancer contexts, where its persistent activation is commonly observed[224–226]. The activation of NF-kB is also associated with the regulation of inflammatory cytokines, which are pivotal in the tumor microenvironment and contribute to the pathogenesis of various cancers[227,228]. Furthermore, NF-kB's involvement in apoptosis regulation highlights its dual role in both promoting cell survival and mediating programmed cell death, depending on the cellular context and stimuli[229,230]. This complex interplay underscores the significance of NF-kB as a therapeutic target in cancer treatment strategies aimed at modulating its activity to influence tumor behavior[211,231].As a result, these findings suggest that DDMP's inhibition of NF-kB may be a critical mechanism in the inhibition of MDA-MB 231 human TNBC cell growth. The structural diversity of these compounds allows for the exploration of their mechanisms of action, potentially leading to the development of effective therapeutic agents for TNBC treatment.

Another compound identified in our study was 1,2,4-Triazine-3,5(2 H,4 H)-dione, also known as 6-azauracil, is a pyrimidine analogue that has demonstrated significant antitumor effects against various transplantable mouse tumors, as noted by Sorm and Keilova in 1958[232]. Similarly, 6-azauridine, a synthetic analogue of uracil, has shown notable antitumor activity in animal models and has been approved for human clinical trials[233]. The mechanism of action for 6-azauridine involves the inhibition of transcription by depleting intracellular pools of guanosine monophosphate (GMP) and uridine monophosphate (UMP), which is critical for RNA synthesis[234]. This depletion disrupts the nucleotide balance necessary for cellular proliferation, thereby exerting its antitumor effects[235]. The development of these pyrimidine analogues highlights their potential in cancer therapy, particularly in targeting metabolic pathways essential for tumor growth[236]. The compound's ability to induce apoptosis and inhibit cell proliferation in TNBC cells has been documented, suggesting a promising role in combination therapies[237,238]. Given the urgent need for effective treatments for TNBC, ongoing research into the use of 6-azauracil could provide valuable insights into novel therapeutic strategies[239,240].Another compound we identified in the water-soluble extract is the naturally occurring compound α-pinene is able to inhibit the cell cycle transition from the G2 to the M phase[241,242]. It has been proposed that α-pinene-induced cell-cycle arrest is regulated by the CDKN1B/p27-CDK1 signaling pathway, as well as by Chk2 and CDC25C[168,241,242].The isolated compound pyrrolidine has been shown to induce G0/G1 cell cycle arrest and time- and dose-dependent cellular apoptosis in both HCT116 and HL60 cells, suggesting that this type of pyrrolidine structure could be a promising candidate for future anticancer therapies[243,244]. Recent studies have demonstrated that pyrrolidine derivatives exhibit significant pro-apoptotic effects, particularly in colorectal cancer cell lines, by activating both intrinsic and extrinsic apoptotic pathways[243]. Furthermore, the induction of oxidative stress by pyrrolidine compounds has been linked to enhanced apoptosis, indicating a potential mechanism through which these compounds exert their anticancer effects[244]. The evidence supports the notion that pyrrolidine-based structures may serve as effective therapeutic agents in the treatment of colorectal cancer and other malignancies[244]. pyrrolidine represent a promising class of compounds in the sht against triple-negative breast cancer. Their demonstrated cytotoxicity against TNBC cell lines, coupled with their ability to induce apoptosis and possibly modulate tumor microenvironment factors, underscores the need for further research into their mechanisms of action and therapeutic potential. Continued exploration of these compounds may lead to the development of novel treatment strategies for this challenging subtype of breast cancer. The compound schizandrin may also increase doxorubicin-induced apoptosis in cancer cells by activating the mitochondrial apoptotic pathway without causing obvious toxicity to normal cells[245,246], as well as inhibit ATR protein kinase activity in response to DNA damage[233,247]. For lung cancer, Schisandrin hinders the proliferation of lung adenocarcinoma A549 cells by promoting cell cycle arrest and apoptosis[99,248].

Western blot analysis of Schizandrin-treated A549 cells revealed an increase in pro-apoptotic markers such as Bax, cleaved caspase-9, cleaved caspase-3, and cleaved PARP, alongside a decrease in the anti-apoptotic protein Bcl-2, indicating a shift towards apoptosis[249]. Additionally, Schizandrin treatment resulted in elevated levels of p53, a critical regulator of cell cycle arrest and apoptosis, which is consistent with findings that p53 activation leads to increased expression of pro-apoptotic genes and cell cycle inhibitors[250,251]. The downregulation of NF-κB, cyclin D1, and CDK-4 further supports the notion that Schizandrin exerts its effects by disrupting cell proliferation pathways, promoting apoptosis in cancer cells[249]. In the context of TNBC, the combination of traditional chemotherapeutic agents with natural compounds like schizandrin may enhance therapeutic efficacy. Current treatment strategies for TNBC often involve DNA-damaging agents and targeted therapies; however, resistance to these treatments is common[252,253]. The incorporation of schizandrin could potentially overcome some of this resistance by enhancing the sensitivity of TNBC cells to chemotherapy through its cytoprotective and anti-apoptotic effects[254,255]. Moreover, the anti-cancer properties of schizandrin have been linked to its ability to inhibit tumor growth and induce apoptosis in various cancer cell lines, indicating its promise as a

complementary therapeutic agent in TNBC management[256,257]. The compound identified as being similar to the synthetic compound, taurolidine, present in the water-soluble *T. violacea* extract, may like taurolidine be a chemotherapeutic agent that methylates the amino groups of cell surface proteins and is thought to be extremely effective in inflammatory diseases[258]. The results of studying the effects of taurolidine on tumor cell apoptosis would indicate that lower concentrations of taurolidine (5 g/mL and 10 g/mL) promote tumor cell apoptosis, whereas higher concentrations (15 g/mL and 25 g/mL) promote cell necrosis[259–262]. Taurolidine's mechanism of action includes the modulation of pro-inflammatory cytokines, such as tumor necrosis factor-alpha (TNF-α), which is known to influence apoptosis pathways[263,264]. The compound has demonstrated efficacy in inhibiting tumor growth and enhancing the apoptotic process through various pathways, including the activation of caspases and the disruption of mitochondrial integrity[261,265]. Overall, taurolidine's dual role as an anti-inflammatory and anti-neoplastic agent positions it as a valuable therapeutic option in cancer treatment. In conclusion, taurolidine presents a multifaceted approach to combating triple-negative breast cancer, characterized by its ability to induce apoptosis, inhibit angiogenesis, and maintain a favorable safety profile. Further research is warranted to elucidate its mechanisms of action and to explore its efficacy in clinical settings specifically targeting TNBC. Cuminaldehyde (Benzaldehyde,4-(-1-methylethyl)) has been shown to induce apoptosis and inhibit cell growth through mechanisms involving mitochondrial dysfunction, specifically by depleting mitochondrial membrane potential (ΔΨm) and activating caspases. The depletion of ΔΨm is critical in triggering the release of pro-apoptotic factors such as cytochrome c, which subsequently activates the caspase cascade, particularly caspase-3 and caspase-9, leading to apoptosis[266,267]. This process is supported by findings that alterations in mitochondrial function, including the generation of reactive oxygen species (ROS), are associated with the induction of apoptosis[268,269]. Moreover, cuminaldehyde's ability to modulate mitochondrial dynamics and promote oxidative stress further corroborates its role in apoptosis[270,271]. Thus, the evidence suggests that cuminaldehyde's anticancer properties are closely linked to its impact on mitochondrial integrity and function. Cuminaldehyde represents a promising area of research in the context of TNBC due to its potential apoptotic effects and the urgent need for new therapeutic strategies for this aggressive cancer subtype. Further studies are warranted to elucidate its mechanisms of action and to evaluate its efficacy in clinical settings.

Oxime and methoxy-phenyl compounds have emerged as promising anti-cancer agents due to their ability to modulate various biological pathways. For instance, oxime derivatives, such as TFOBO, have been shown to induce cell death in myeloid leukemia by modulating reactive oxygen species and NADPH oxidase activity, highlighting their potential in targeting cancer cells through oxidative stress mechanisms[272]. Furthermore, methoxy-substituted compounds have been associated with enhanced anti-cancer activity. For example, methoxy groups on flavanone derivatives have been linked to increased cell permeability and apoptosis in cancer cell lines[273]. Additionally, methoxy-phenyl derivatives have demonstrated significant cytotoxic effects against various cancer types, including breast cancer[274]. The presence of methoxy groups appears to enhance the biological activity of these compounds, making them valuable candidates for further development in cancer therapeutics[275].

In conclusion, the exploration of oxime and methoxy-phenyl compounds as therapeutic agents for triple-negative breast cancer represents a promising avenue for research. Their ability to induce apoptosis, modulate oxidative stress, and potentially alter the tumor microenvironment positions them as valuable candidates in the ongoing battle against this aggressive cancer subtype. Future studies should focus on elucidating the specific mechanisms of action of these compounds and their effectiveness in clinical settings.

Vanillin, a phenomenon, has garnered attention for its potential anti-cancer properties. Research indicates that vanillin exhibits anti-neoplastic effects, particularly through mechanisms such as the inhibition of cell proliferation and migration in various cancer types, including melanoma and cervical cancer[276,277]. Its ability to modulate key signaling pathways, such as NF-κB and HIF-1α, contributes to its anti-invasive and anti-metastatic actions[276,278]. Additionally, vanillin has demonstrated antioxidant and anti-inflammatory properties, which may further enhance its therapeutic efficacy against cancer[279,280]. Studies have also shown that vanillin can induce apoptosis in cancer cells, thereby reducing tumor growth[281]. Overall, the multifaceted biological activities of vanillin position it as a promising candidate for cancer prevention and treatment strategies. In summary, vanillin presents a promising avenue for the treatment of triple-negative breast cancer through its multifaceted mechanisms, including the inhibition of cell proliferation, modulation of cancer stem cell properties, induction of apoptosis, and interference with critical signaling pathways. As research continues to elucidate the specific pathways and molecular interactions involved, vanillin may serve as a valuable component in the development of novel therapeutic strategies for TNBC.

D-Glycero-D-galacto-heptose has shown potential as an anti-cancer compound, particularly in the context of triple-negative breast cancer (TNBC). This heptose sugar is involved in the biosynthesis of lipopolysaccharides (LPS) and has been identified as a pathogen-associated molecular pattern (PAMP) that can stimulate immune responses[282,283]. Research indicates that D-glycero-D-galacto-heptose can enhance the activation of immune cells, which may contribute to the inhibition of tumor growth and metastasis in TNBC models[284,285]. Moreover, studies have demonstrated that derivatives of D-glycero-D-galacto-heptose can inhibit the proliferation and migration of cancer cells, including those from glioma and potentially TNBC[286,287]. The structural characteristics of this compound allow it to interact with various immune receptors, suggesting its utility in cancer immunotherapy[288]. Thus, the exploration of D-glycero-D-galacto-heptose as a therapeutic agent against TNBC represents a promising area for further research.

It is noteworthy that the same compounds were capable of binding both isoforms, although with lower affinity for COX-1. These findings suggest that the anticancer activity of T. violacea compounds may be mediated by their preferential binding to COX-2, which is often upregulated in cancers. The binding scores indicate that D-Glycero-d-galacto-heptose bind with much higher affinity to COX-2 than to COX-1. COX-2 demonstrated the highest average docking scores, indicating stronger binding affinity for the T. violacea-derived compounds.

Comparative structural analysis revealed significant differences in binding site residues and global backbone structures between COX-1 and COX-2. SiteMap analysis identified the most druggable regions, with COX-2's larger binding pocket enabling higher binding affinity.

The increase in the transcription of pro-apoptotic genes in TNBC cells following treatment is not unexpected, firstly, due to the increase in apoptosis as indicated by the apoptosis assay, and secondly, as the molecular make-up of the extract was shown to consist of multiple compounds that are known to induce apoptosis, and it is likely that these very different compounds would act in different ways to induce apoptosis. The anti-apoptotic genes show an equal amount of increased and decreased transcription in TNBC cells following treatment. However, two members of the intrinsic pathway are downregulated.

The lesser increase in apoptosis observed in the normal cells following treatment with the water-soluble *T. violacea* extract is reflected by the transcript changes shown in Fig. 8A and B. Once again, the level of most pro-apoptotic gene transcription is increased following treatment. However, there is also an increase in the level of many anti-apoptotic genes. The extremely high level of transcripts for these genes may indicate the activation of anti-apoptotic pathways to counteract the induction of apoptosis due to the presence of the extract, resulting in lower levels of apoptosis. The S phase arrest induced by treatment with the *T. violacea* water soluble extract observed in both TNBC and normal cells as observed in the cell cycle assay which led to an accumulation of cells in the S phase in both cell types resulted in a comparison of the fold changes in the transcript level of genes that promote S phase progression as well as those that promote S phase arrest. The transcriptome changes we observe reflect the S phase arrest observed following treatment. In the TNBC cell line (Fig. 8C and D) here is a clear increase in the transcription of genes that could lead to an S-phase arrest. The situation is not as clear in normal breast cells, and this may explain why the extract has less severe deleterious effects on the growth of the normal cells.

Conclusions

Water-soluble extracts of the medicinal plant *Tulbaghia violacea* demonstrated selective cytotoxic activity against the TNBC cell line MDA-MB231 with an IC50 value of 395 µg/mL. While these IC50 values are classified as "low activity" according to the WHO guidelines for medicinal plant extracts, it is important to note that crude extracts often contain a mixture of bioactive and inactive compounds, which can dilute the observed cytotoxic effects. Despite this limitation, the extract selectively induced apoptosis in TNBC cells and caused S-phase cell cycle arrest, with a minimal impact on normal breast cells at sub-IC50 concentrations. These results suggest that the bioactive constituents of T. violacea have potential for further development as anti-cancer agents, particularly after purification, to isolate the active compounds and improve their potency. However, the methanol-soluble extract exhibited higher IC50 values (820 µg/mL), indicating lower activity. This may have been due to solubility challenges, as the extract could not be fully dissolved in cell culture medium containing 0.5% DMSO. Addressing these solubility issues in future studies may reveal stronger activity of the methanol-soluble fraction. Further research should focus on optimizing extraction methods, purifying bioactive compounds, and investigating their molecular targets and mechanisms of action. These efforts will help to determine the therapeutic potential of T. violacea and its bioactive constituents more accurately.

In conclusion, the author should try analyze the expression/suppression of genes before and after treatment ad corelate these with different pathological processes involved in cancer and cell death. She mentioned genes involved in apoptosis and discussed these, but did not discuss the ones in the study considering their expression/suppression.

The water-soluble extracts of *Tulbaghia violacea* demonstrated selective cytotoxic activity against the TNBC cell line MDA-MB231. Transcriptomic analysis revealed significant changes in the expression of genes involved in critical cancer-related pathways before and after treatment. Pro-apoptotic genes such as BAX, CASP3, and TP53 were upregulated, supporting the induction of apoptosis as a primary mechanism of cell death. Conversely, the suppression of anti-apoptotic genes such as BCL2 and MCL1 highlights the extract's potential to disrupt survival signalling in TNBC cells.

Beyond apoptosis, the extract modulated the expression of genes involved in cell cycle regulation, including the upregulation of genes associated with S-phase arrest (CDKN1A) and the suppression of genes promoting cell cycle progression (CCND1, CDK4). These findings suggest that the extract not only induces apoptosis but also inhibits proliferation by disrupting cell cycle dynamics, further contributing to its anti-cancer effects.

These results provide insights into the molecular mechanisms underlying the extract's cytotoxicity and emphasize its potential as a source of bioactive compounds targeting multiple pathological processes in cancer. Future studies will aim to validate these pathways and explore their therapeutic relevance in cancer treatment.

Data availability

The original data presented in the study are openly available in the Sequence Read Archive (SRA) submission: SUB14608306 available through NCBI servers.

Received: 3 July 2024; Accepted: 28 January 2025
Published online: 17 February 2025

References

1. Dent, R. et al. Pattern of metastatic spread in triple-negative breast cancer. *Breast Cancer Res. Treat.* **115**(2), 423–428 (2009).
2. Carey, L. A. et al. The triple negative paradox: primary tumor chemosensitivity of breast cancer subtypes. *Clin. Cancer Res.* **13**(8), 2329–2334 (2007).
3. Shin, V. Y. et al. Circulating cell-free miRNAs as biomarker for triple-negative breast cancer. *Br. J. Cancer*. **112**(11), 1751–1759 (2015).

4. Dent, R. et al. Triple-negative breast cancer: clinical features and patterns of recurrence. *Clin. Cancer Res.* **13**(15 Pt 1), 4429–4434 (2007).
5. Boyle, P. Triple-negative breast cancer: epidemiological considerations and recommendations. *Ann. Oncol.* **23**(Suppl 6), vi7–12 (2012).
6. Foulkes, W. D., Smith, I. E. & Reis-Filho, J. S. Triple-negative breast cancer. *N Engl. J. Med.* **363**(20), 1938–1948 (2010).
7. Bauer, K. R. et al. Descriptive analysis of estrogen receptor (ER)-negative, progesterone receptor (PR)-negative, and HER2-negative invasive breast cancer, the so-called triple-negative phenotype: a population-based study from the California cancer Registry. *Cancer* **109**(9), 1721–1728 (2007).
8. Carey, L. A. et al. Race, breast cancer subtypes, and survival in the Carolina breast Cancer Study. *Jama* **295**(21), 2492–2502 (2006).
9. Lara-Medina, F. et al. Triple-negative breast cancer in hispanic patients: high prevalence, poor prognosis, and association with menopausal status, body mass index, and parity. *Cancer* **117**(16), 3658–3669 (2011).
10. Millikan, R. C. et al. Epidemiology of basal-like breast cancer. *Breast Cancer Res. Treat.* **109**(1), 123–139 (2008).
11. Shinde, S. S. et al. Higher parity and shorter breastfeeding duration: association with triple-negative phenotype of breast cancer. *Cancer* **116**(21), 4933–4943 (2010).
12. Fostira, F. et al. Prevalence of BRCA1 mutations among 403 women with triple-negative breast cancer: implications for genetic screening selection criteria: a Hellenic Cooperative Oncology Group Study. *Breast Cancer Res. Treat.* **134**(1), 353–362 (2012).
13. Richardson, L. C. et al. Patterns and trends in Age-Specific Black-White differences in breast Cancer incidence and mortality - United States, 1999–2014. *MMWR Morb Mortal. Wkly. Rep.* **65**(40), 1093–1098 (2016).
14. Newman, L. A. et al. Association between Benign breast disease in African American and white American women and subsequent triple-negative breast Cancer. *JAMA Oncol.* **3**(8), 1102–1106 (2017).
15. André, F. & Zielinski, C. C. Optimal strategies for the treatment of metastatic triple-negative breast cancer with currently approved agents. *Ann. Oncol.* **23**(Suppl 6), vi46–51 (2012).
16. Citron, M. L. et al. Randomized trial of dose-dense versus conventionally scheduled and sequential versus concurrent combination chemotherapy as postoperative adjuvant treatment of node-positive primary breast cancer: first report of Intergroup Trial C9741/Cancer and Leukemia Group B Trial 9741. *J. Clin. Oncol.* **21**(8), 1431–1439 (2003).
17. Hayes, D. F. et al. HER2 and response to paclitaxel in node-positive breast cancer. *N Engl. J. Med.* **357**(15), 1496–1506 (2007).
18. Berry, D. A. et al. Estrogen-receptor status and outcomes of modern chemotherapy for patients with node-positive breast cancer. *Jama* **295**(14), 1658–1667 (2006).
19. Liu, M. M., Huang, Y. & Wang, J. Developing phytoestrogens for breast cancer prevention. *Anticancer Agents Med. Chem.* **12**(10), 1306–1313 (2012).
20. Zhang, Y. et al. Phytochemicals of garlic: promising candidates for cancer therapy. *Biomed. Pharmacother.* **123**, 109730 (2020).
21. Caputi, L. et al. Missing enzymes in the biosynthesis of the Anticancer Drug Vinblastine in Madagascar Periwinkle. *Science* **360**(6394), 1235–1239 (2018).
22. Chagas, C. M. & Alisaraie, L. Metabolites of Vinca Alkaloid Vinblastine: tubulin binding and activation of nausea-Associated receptors. *ACS Omega.* **4**(6), 9784–9799 (2019).
23. Qu, Y., Сафонова, О. А. & Luca, V. D. Completion of the Canonical Pathway for Assembly of Anticancer Drugs Vincristine/Vinblastine in <i>Catharanthus Roseus. *Plant J.* **97**(2), 257–266 (2018).
24. Rahim, A. A. et al. Determination and quantification of the Vinblastine content in Purple, Red, and White Catharanthus Roseus leaves using RP-HPLC method. *Adv. Pharm. Bull.* **8**(1), 157–161 (2018).
25. Mans, D. R., da Rocha, A. B. & Schwartsmann, G. Anti-cancer drug discovery and development in Brazil: targeted plant collection as a rational strategy to acquire candidate anti-cancer compounds. *Oncologist* **5**(3), 185–198 (2000).
26. Mohan, S. et al. Involvement of NF-κB and Bcl2/Bax signaling pathways in the apoptosis of MCF7 cells induced by a xanthone compound pyranocycloartobiloxanthone A. *Phytomedicine* **19**(11), 1007–1015 (2012).
27. Yang, B. et al. Pharmacokinetic comparison of seven major bioactive components in normal and depression model rats after oral administration of Baihe Zhimu decoction by liquid chromatography-tandem mass spectrometry. *J. Pharm. Biomed. Anal.* **148**, 119–127 (2018).
28. Jin, J. et al. Capsaicin mediates cell cycle arrest and apoptosis in human colon cancer cells via stabilizing and activating p53. *Int. J. Biol. Sci.* **10**(3), 285–295 (2014).
29. Van Wyk, B. E., Oudtshoorn, B. & Gericke, N. *Medicinal Plants of South Africa* (Briza, 1997).
30. Motadi, L. R., Choene, M. S. & Mthembu, N. N. Anticancer properties of Tulbaghia Violacea regulate the expression of p53-dependent mechanisms in cancer cell lines. *Sci. Rep.* **10**(1), 12924 (2020).
31. Takaidza, S. et al. Anticancer activity of crude acetone and water extracts of Tulbaghia violacea on human oral cancer cells. *Asian Pac. J. Trop. Biomed.* **8**(9), 456 (2018).
32. Saibu, G. M. et al. In vitro cytotoxic and pro-apoptotic effects of water extracts of Tulbaghia violacea leaves and bulbs. *J. Ethnopharmacol.* **164**, 203–209 (2015).
33. Abubakar, A. R. & Haque, M. Preparation of Medicinal plants: basic extraction and fractionation procedures for experimental purposes. *J. Pharm. Bioallied Sci.* **12**(1), 1–10 (2020).
34. Zhang, Q. W., Lin, L. G. & Ye, W. C. Techniques for extraction and isolation of natural products: a comprehensive review. *Chin. Med.* **13**, 20 (2018).
35. Warnis, M., Yulinda, T. & Maryanti, L. Comparison of the antioxidant activity of Cashew (*Nacardium Occidentale* L.) Leaf Extract with the soxhletation and reflux extraction methods (2021).
36. Yasir, B. & Rohman, A. Optimization of Pagoda (Clerodendrum Paniculatum L.) extraction based by Analytical Factorial Design Approach, its phytochemical compound, and cytotoxicity activity. *Egypt. J. Chem.* **0**(0), 0–0 (2022).
37. Idoudi, S. et al. Influence of extraction techniques and solvents on the antioxidant and biological potential of different parts of Scorzonera Undulata. *Life (Basel)* **13**(4) (2023).
38. Amaro, F. et al. β-Adrenoceptor activation in breast MCF-10A cells induces a pattern of catecholamine production similar to that of tumorigenic MCF-7 cells. *Int. J. Mol. Sci.* **21**(21) (2020).
39. Larsson, P. et al. Optimization of cell viability assays to improve replicability and reproducibility of cancer drug sensitivity screens. *Sci. Rep.* **10**(1), 5798 (2020).
40. Rampersad, S. N. Multiple applications of Alamar Blue as an indicator of metabolic function and cellular health in cell viability bioassays. *Sens. (Basel).* **12**(9), 12347–12360 (2012).
41. Khan, M. M. et al. Osteogenic induction with Silicon Hydroxyapatite using modified autologous adipose tissue-derived stromal vascular fraction: in Vitro and qualitative histomorphometric analysis. *Mater. (Basel)* **15**(5) (2022).
42. Alsubait, S. A. et al. Cytotoxicity of different concentrations of three Root Canal Sealers on Human mesenchymal stem cells. *Biomolecules* **8**(3) (2018).
43. Jafari, A. et al. Evaluation of accuracy of microplate alamar blue assay and proportion method for prompt detection of Mycobacterium tuberculosis and clinical isolates of multidrug-resistant M. tuberculosis. **14**(3) (2021).
44. Méndez-González, V. M. et al. Biocompatibility of Bioactive Sealers Bio-C Sealer vs MTA repair HP in human fibroblasts 59–68 (2024).
45. Atienzar, F. A. et al. Evaluation of impedance-based label-free technology as a tool for pharmacology and toxicology investigations. *Biosens. (Basel).* **3**(1), 132–156 (2013).

46. Stefanowicz–Hajduk, J. et al. Reuse of E-Plate cell sensor arrays in the xCELLigence Real-Time Cell Analyzer. *Biotechniques* **61**(3), 117–122 (2016).
47. ŞAhİN, Y. Cytotoxic and antiproliferative effects of Hellebrin on breast and Lung Cancer cells. *Veteriner Hekimler Derneği Dergisi*. **94**(2), 137–143 (2023).
48. Pal, R. et al. Diverse effects of dimethyl sulfoxide (DMSO) on the differentiation potential of human embryonic stem cells. *Arch. Toxicol.* **86**(4), 651–661 (2012).
49. Jamalzadeh, L. et al. Cytotoxic effects of some common organic solvents on MCF-7, RAW-264.7 and human umbilical vein endothelial cells (2016).
50. Lee, Y. J., Park, K. S. & Lee, S. H. Curcumin targets both apoptosis and necroptosis in acidity-tolerant prostate carcinoma cells. *Biomed. Res Int* **2021**, 8859181 (2021).
51. Darzynkiewicz, Z., Huang, X. & Zhao, H. Analysis of cellular DNA content by flow cytometry. *Curr. Protoc. Cytom* **82**, 7.5.1–7.5.20 (2017).
52. Lim, S. & Kaldis, P. Cdks, cyclins and CKIs: roles beyond cell cycle regulation. *Development* **140**(15), 3079–3093 (2013).
53. Gerena, Y., González-Pons, M. & Serrano, A. E. Cytofluorometric Detection of Rodent Malaria Parasites using red-excited fluorescent dyes. *Cytometry Part. A*. **79A**(11), 965–972 (2011).
54. Chang, M. C. et al. Effects of Camphorquinone on cytotoxicity, cell cycle regulation and prostaglandin E2 production of Dental Pulp cells: role of ROS, ATM/Chk2, MEK/ERK and Hemeoxygenase-1. *PLoS One*. **10**(12), e0143663 (2015).
55. Qi, F. & Zhang, F. Cell cycle regulation in the plant response to stress. *Front. Plant Sci.* **10** (2020).
56. Nelson, J. et al. Relationship between membrane permeability and specificity of human secretory phospholipase A(2) isoforms during cell death. *Biochim. Biophys. Acta*. **1808**(7), 1913–1920 (2011).
57. Al-Dabbagh, B. et al. Antioxidant and anticancer activities of Trigonella Foenum-Graecum, Cassia Acutifolia and Rhazya Stricta. *BMC Complement. Altern. Med.* **18**(1) (2018).
58. Almeida-Terassi, L. M. Cytogenotoxic screening of the natural compound niga-ichigoside F1 from <i>Rubus Imperialis (Rosaceae). *J. Appl. Toxicol.* **44**(8), 1129–1138 (2024).
59. Zhang, B. et al. An Inexpensive High-Throughput Nuclear magnetic resonance tube cleaning Apparatus. *Anal. Biochem.* **416**(2), 234–236 (2011).
60. Xu, J. et al. Metabolic response in rats following electroacupuncture or moxibustion stimulation. **2019**(1), 6947471 (2019).
61. Vreven, T. et al. Performance of ZDOCK and IRAD in CAPRI rounds 28–34. *Proteins* **85**(3), 408–416 (2017).
62. Fan, N. et al. Docking Approach augmented by machine learning for protein structure selection yields Superior virtual screening performance. *Mol. Inf.* **39**(4), e1900103 (2020).
63. Buermans, H. P. et al. New methods for next generation sequencing based microRNA expression profiling. *BMC Genom.* **11**, 716 (2010).
64. Lear, G. et al. Methods for the extraction, storage, amplification and sequencing of DNA from environmental samples. Nz (2018).
65. Pecman, A. et al. Systematic comparison of Nanopore and Illumina Sequencing for the Detection of Plant Viruses and viroids using total RNA sequencing Approach. *Front. Microbiol.* **13**, 883921 (2022).
66. Lw, A. et al. Extraction from primary liquid blood cultures for bloodstream infection diagnosis using whole genome sequencing. *J. Med. Microbiol.* **67**(3), 347–357 (2018).
67. Tafakh, M. S. et al. Sulforaphane, a Chemopreventive Compound, inhibits Cyclooxygenase-2 and microsomal prostaglandin E Synthase-1 expression in human HT-29 Colon cancer cells. *Cells Tissues Organs.* **206**(1–2), 46–53 (2018).
68. Xing, J. S. et al. Isoalantolactone inhibits IKKβ kinase activity to interrupt the NF-κB/COX-2-mediated signaling cascade and induces apoptosis regulated by the mitochondrial translocation of cofilin in glioblastoma. *Cancer Med.* **8**(4), 1655–1670 (2019).
69. Che, L. et al. Targeting mitochondrial COX-2 enhances chemosensitivity via Drp1-dependent remodeling of mitochondrial dynamics in hepatocellular carcinoma. *Cancers (Basel)* **14**(3) (2022).
70. Han, B. et al. Study on the physical and chemical properties of dimethyl sulfoxide under the external electric field. *Phys. Scr.* **98**(11), 115011 (2023).
71. Deguchi, Y. et al. Study on autocatalytic decomposition of dimethyl sulfoxide (DMSO). **24**(9), 1614–1620 (2020).
72. Wood-Black, F. et al. *Highlights: Correlating Molecular Structures to Physical Properties, Ammonium Nitrate in the News, Tools and Databases, and More: Submit Contributions to highlights@ Safety. acs. org and be Coauthored, or Share Ideas on Social Media with# SafetyHighlights* (ACS, 2020).
73. Abdelkefi, A. et al. Severe neurotoxicity associated with dimethyl sulphoxide following PBSCT. *Bone Marrow Transpl.* **44**(5), 323–324 (2009).
74. Peplow, M. Cryo-Electron Microscopy reaches Resolution Milestone. *ACS Cent. Sci.* **6**(8), 1274–1277 (2020).
75. Tian, Y. et al. High pressure/temperature pasting and gelling of starch related to multilevel structure-analyzed with RVA 4800. *Carbohydr. Polym.* **295**, 119858 (2022).
76. Liu, Y. et al. The intra-S phase checkpoint directly regulates replication elongation to preserve the integrity of stalled replisomes. *Proc. Natl. Acad. Sci. U S A* **118**(24) (2021).
77. Aremu, A. O. & Van Staden, J. The genus Tulbaghia (Alliaceae)—A review of its ethnobotany, pharmacology, phytochemistry and conservation needs. *J. Ethnopharmacol.* **149**(2), 387–400 (2013).
78. Feng, Y. et al. Breast cancer development and progression: risk factors, cancer stem cells, signaling pathways, genomics, and molecular pathogenesis. *Genes Dis.* **5**(2), 77–106 (2018).
79. Bouyahya, A. et al. In vitro antiproliferative activity of selected medicinal plants from the North-West of Morocco on several cancer cell lines. *Eur. J. Integr. Med.* **18**, 23–29 (2018).
80. Nair, J. J. et al. Antibacterial constituents of the plant family Amaryllidaceae. *Bioorg. Med. Chem. Lett.* **27**(22), 4943–4951 (2017).
81. León, K. A. et al. Alkaloids of Phaedranassa Dubia (Kunth) J.F. Macbr. And Phaedranassa Brevifolia Meerow (Amaryllidaceae) from Ecuador and its cholinesterase-inhibitory activity. *S Afr. J. Bot.* **136**, 91–99 (2021).
82. Hao, B., Shen, S. F. & Zhao, Q. J. Cytotoxic and antimalarial amaryllidaceae alkaloids from the bulbs of Lycoris radiata. *Molecules* **18**(3), 2458–2468 (2013).
83. Duan, Z. W. et al. [Non-alkaloid constituents of Hymenocallis littoralis]. *Zhongguo Zhong Yao Za Zhi*. **46**(20), 5304–5309 (2021).
84. Ibrakaw, A. S. et al. Neuroprotective activities of Boophone haemanthoides (Amaryllidaceae) Extract and its Chemical constituents. *Molecules* **25**(22) (2020).
85. Matsuura, H. N. & Fett-Neto, A. G. in *Plant Alkaloids: Main Features, Toxicity, and Mechanisms of Action* 1–15 (eds Toxins, P.et al.) (Springer Netherlands, 2015).
86. Ban, J. O. et al. Anti-proliferate and pro-apoptotic effects of 2,3-dihydro-3,5-dihydroxy-6-methyl-4H-pyranone through inactivation of NF-kappaB in human colon cancer cells. *Arch. Pharm. Res.* **30**(11), 1455–1463 (2007).
87. Ahmad, K. et al. Antioxidant and apoptotic effects of Callistemon lanceolatus leaves and their compounds against human cancer cells. *Biomed. Pharmacother.* **106**, 1195–1209 (2018).
88. Shukla, R. et al. Antioxidant and antiapoptotic effect of aqueous extract of Pueraria tuberosa (Roxb. Ex Willd.) DC. On streptozotocin-induced diabetic nephropathy in rats. **18**(1), 1–11 (2018).
89. Abarca-Vargas, R., Peña, C. F., Malacara & Petricevich, V. L. Characterization of Chemical compounds with antioxidant and cytotoxic activities in Bougainvillea x Buttiana Holttum and Standl, (var. Rose) extracts. *Antioxidants (Basel)* **5**(4) (2016).
90. Sorm, F., Jakubovic, A. & Slechta, L. The anticancerous action of 6-azauracil (3, 5-dioxo-2, 3, 4, 5-tetrahydro-1, 2, 4-triazine). *Experientia* **12**(7), 271–272 (1956).

91. Sorm, F. & Keilova, H. The anti-tumour activity of 6-azauracil riboside. *Experientia* **14**(6), 215 (1958).
92. Betz, J. L. et al. Phenotypic analysis of Paf1/RNA polymerase II complex mutations reveals connections to cell cycle regulation, protein synthesis, and lipid and nucleic acid metabolism. *Mol. Genet. Genomics.* **268**(2), 272–285 (2002).
93. Liang, L. et al. Nonhydrolyzable Heptose Bis- and Monophosphate Analogues modulate pro-inflammatory TIFA-NF-κB signaling. *Chembiochem* **21**(20), 2982–2990 (2020).
94. Tsai, K. D. et al. Cuminaldehyde from Cinnamomum verum induces cell death through Targeting Topoisomerase 1 and 2 in human colorectal adenocarcinoma COLO 205 cells. *Nutrients* **8**(6) (2016).
95. Yan, Y. Q. et al. Vanillin derivative 6-bromine-5-hydroxy-4-methoxybenzaldehyde-elicited apoptosis and G2/M arrest of jurkat cells proceeds concurrently with DNA-PKcs cleavage and akt inactivation. *Int. J. Oncol.* **29**(5), 1167–1172 (2006).
96. Cheng, W. Y. et al. Microarray analysis of vanillin-regulated gene expression profile in human hepatocarcinoma cells. *Pharmacol. Res.* **56**(6), 474–482 (2007).
97. Ji, J. et al. Synthesis and biological evaluation of substituted pyrrolidines and pyrroles as potential anticancer agents. *Arch. Pharm. (Weinheim).* **353**(12), e2000136 (2020).
98. Li, S. et al. Schisandrin B inhibits epithelial–mesenchymal transition and stemness of large–cell lung cancer cells and tumorigenesis in xenografts via inhibiting the NF–κB and p38 MAPK signaling pathways. *Oncol. Rep.* **45**(6) (2021).
99. Lv, X. J. et al. Schisandrin B inhibits the proliferation of human lung adenocarcinoma A549 cells by inducing cycle arrest and apoptosis. *Int. J. Clin. Exp. Med.* **8**(5), 6926–6936 (2015).
100. Duan, X. et al. Terbutaline attenuates LPS-induced injury of pulmonary microvascular endothelial cells by cAMP/Epac signaling. *Drug Dev. Res.* **83**(3), 699–707 (2022).
101. Cowan, M. Home care of the pregnant woman using terbutaline. *MCN Am. J. Matern Child. Nurs.* **18**(2), 99–105 (1993).
102. Zelman, S. Terbutaline and muscular symptoms. *Jama* **239**(10), 930 (1978).
103. Ismail, M. I. et al. Targeting multiple conformations of SARS-CoV2 Papain-Like protease for drug repositioning: an in-silico study. *Comput. Biol. Med.* **131**, 104295 (2021).
104. Miñano, F. J. & Myers, R. D. Inhibition of brain dopa-decarboxylase by RO 4-4602 infused ICV blocks alcohol drinking induced in rats by cyanamide. *Psychopharmacol. (Berl).* **98**(2), 176–182 (1989).
105. Raghav, S. Perju-Dumbrava, and Rehabilitation, Treatment of Parkinson's Disease 105–117 (2022).
106. Paul, A. Antidiarrheal agents. *Introduction to Basics of Pharmacology Toxicology: Volume 2: Essentials of Systemic Pharmacology: From Principles to Practice* 605–611 (2021).
107. Matin, M. A., Jaffery, F. N. & Kar, P. P. Role of striatal acetylcholine and free ammmonia in the central stimulatory effects of pp'DDT in rats. Protective effects of barbiturates. *Arch. Toxicol.* **45**(1), 29–35 (1980).
108. Refat, M. S. et al. Synthesis of N,N'-bis(1,5-dimethyl-2-phenyl-1,2-dihydro-3-oxopyrazol-4-yl) sebacamide that ameliorate osteoarthritis symptoms and improve bone marrow matrix structure and cartilage alterations induced by monoiodoacetate in the rat model: suggested potent anti-inflammatory agent against COVID-19. *Hum. Exp. Toxicol.* **40**(2), 325–341 (2021).
109. Tanaka, E. & Nakamura, K. Comparison of trimethadione and antipyrine as indicators of oxidative drug metabolizing capacity in man. *Eur. J. Clin. Pharmacol.* **36**(6), 629–632 (1989).
110. Edeki, T., Johnston, A. & Turner, P. An examination of a possible pharmacokinetic interaction between nifedipine and antipyrine. *Eur. J. Clin. Pharmacol.* **39**(4), 405–407 (1990).
111. Pawlak, S. et al. Treatment of Pediatric patients with COVID infection after heart transplantation. *Transpl. Proc.* **54**(4), 905–907 (2022).
112. Parkes, J. Clinical Pharmacology of Amantadine and Derivatives. In *Early Diagnosis and Preventive Therapy in Parkinson's Disease* (Springer, 1989).
113. Hammoudi Halat, D. et al. A focused insight into Thyme: Biological, Chemical, and Therapeutic properties of an indigenous Mediterranean Herb. *Nutrients* **14**(10) (2022).
114. Mulubwa, M. & Mugabo, P. Amount of Cycloserine emanating from Terizidone metabolism and relationship with hepatic function in patients with drug-resistant tuberculosis. *Drugs R D.* **19**(3), 289–296 (2019).
115. Wu, H. F. et al. D)-Cycloserine ameliorates Autism-Like deficits by removing GluA2-Containing AMPA receptors in a Valproic Acid-Induced Rat Model. *Mol. Neurobiol.* **55**(6), 4811–4824 (2018).
116. van der Galiën, R. et al. Pharmacokinetic modeling, Simulation, and development of a limited sampling strategy of Cycloserine in patients with Multidrug-/Extensively drug-resistant tuberculosis. *Clin. Pharmacokinet.* **59**(7), 899–910 (2020).
117. Lanthorn, T. H. Agonist turned antagonist. *Amino Acids* **6**(3), 247–260 (1994).
118. Batson, S. et al. Inhibition of D-Ala:D-Ala ligase through a phosphorylated form of the antibiotic D-cycloserine. *Nat. Commun.* **8**(1), p1939 (2017).
119. Ren, S. et al. Hydrocinnamic acid inhibits the currents of WT and SQT3 syndrome-related mutants of Kir2.1 Channel. *J. Membr. Biol.* **250**(5), 425–432 (2017).
120. Bu, R. et al. Autotoxicity in cucumber (Cucumis sativus L.) seedlings is alleviated by silicon through an increase in the activity of antioxidant enzymes and by mitigating lipid peroxidation. **59**, 247–259 (2016).
121. Ryder, N. S. & Mieth, H. Allylamine antifungal drugs. *Curr. Top. Med. Mycol.* **4**, 158–188 (1992).
122. Mühlbacher, J. M. Naftifine: a topical allylamine antifungal agent. *Clin. Dermatol.* **9**(4), 479–485 (1991).
123. Salmoiraghi, I. et al. Allylamine type xanthone antimycotics. *Arch. Pharm. (Weinheim).* **331**(6), 225–227 (1998).
124. Arken, N. Schizandrol A reverses multidrug resistance in resistant chronic myeloid leukemia cells K562/A02. *Cell. Mol. Biol. (Noisy-le-grand).* **65**(1), 78–83 (2019).
125. Brzozowski, Z., Saczewski, F. & Gdaniec, M. Synthesis, molecular structure and anticancer activity of 1-allyl-3-amino-2-(4-chloro-2-mercaptobenzenesulphonyl)guanidine derivatives. *Eur. J. Med. Chem.* **37**(4), 285–293 (2002).
126. van den Hoven, W. E. & Hall, D. W. Inhibition of human platelet functions by cyclandelate. *Drugs* **33**(Suppl 2), 41–52 (1987).
127. Hall, D. W. & van den Hoven, W. E. Influence of cyclandelate on in vitro red blood cell deformability. *Drugs* **33**(Suppl 2), 30–40 (1987).
128. Middleton, B., Cacciaguerra, F. & White, D. Cyclandelate. An inhibitor of cholesterol esterification. *Drugs* **33**(Suppl 2), 75–79 (1987).
129. Ananth, J. Specific effects of cyclandelate on memory. *Drugs* **33**(Suppl 2), 97–102 (1987).
130. Ma, Y. Z., Qiang, G. F., Du, G. H. & Du, G. H. Cyclandelate. in *Natural Small Molecule Drugs from Plants* 227–230 (Springer Singapore, 2018).
131. Bast, A., Leurs, R. & Timmerman, H. Cyclandelate as a calcium modulating agent in rat cerebral cortex. *Drugs* **33**(Suppl 2), 67–74 (1987).
132. Diener, H. C., Kaube, H. & Limmroth, V. Antimigraine drugs. *J. Neurol.* **246**(7): 515–519. (1999).
133. Sharma, R., Trivedi, M. & Trivedi, A. Impact of Space Pharmaceuticals on Cardiovascular System. In *Handbook of Space Pharmaceuticals* 627–643 (Springer, 2022).
134. Boucher, P., Vogel, H. G. & Hock, F. J. Inhibition of Cholesterol Absorption. in *Drug Discovery and Evaluation: Pharmacological Assays* 2273–2281 (Springer International Publishing, 2016).
135. Heise, C. & Brooks, D. *Anxiolytics, Sedatives, and Hypnotics* 935–954 (2017).
136. Parker, F. S. et al. *Applications of Infrared Spectroscopy in Biochemistry, Biology* 390–417 (Springer US, 1971).
137. Smith, J. M. & Misiak, H. Critical flicker frequency (CFF) and psychotropic drugs in normal human subjects-a review. *Psychopharmacologia* **47**(2), 175–182 (1976).

138. Heise, G. A. & Boff, E. Continuous avoidance as a base-line for measuring behavioral effects of drugs. *Psychopharmacologia* **3**, 264–282 (1962).
139. Stedjan, M. K. Augspurger Ring strain energy in ether-and lactone-containing spiro compounds. **28**(4), 298–303 (2015).
140. Omoruyi, B. E., Afolayan, A. J. & Bradley, G. The inhibitory effect of Mesembryanthemum edule (L.) bolus essential oil on some pathogenic fungal isolates. *BMC Complement. Altern. Med.* **14**, 168 (2014).
141. Garg, D., Dar, R. A. & Phutela, U. G. Characterization of novel euryhaline microalgal cultures from Punjab, India for bioactive compounds. *Arch. Microbiol.* **204**(7), 370 (2022).
142. Zheng, A., Dzombak, D. A. & Luthy, R. G. Formation of free cyanide and cyanogen chloride from chloramination of publicly owned treatment works secondary effluent: laboratory study with model compounds. *Water Environ. Res.* **76**(2), 113–120 (2004).
143. Jasser, I. The influence of macrophytes on a phytoplankton community in experimental conditions. *Hydrobiologia* **306**, 21–32 (1995).
144. Kristich, C. J. et al. Esp-independent biofilm formation by Enterococcus faecalis. *J. Bacteriol.* **186**(1), 154–163 (2004).
145. Mahdi, E. A. et al. The impact of glucose and Sodium Chloride on the Biofilm formation of Pseudomonas aeruginosa & Staphylococcus aureus. *J. Pure Appl. Sci.* **33**(4), 1–9 (2020).
146. Moinpour, M. et al. Discriminating changes in protein structure using tyrosine conjugation. *Protein Sci.* **29**(8), 1784–1793 (2020).
147. Saitoh, J. & Saya, H. Benzaldehyde inhibits the multiple signals in cancer by suppressing the binding activity of overexpressed 14-3-3ζ and represses the pRb/E2F transcriptional pathway. *Cancer Res.* **78**(13_Supplement), 2874–2874 (2018).
148. Sinha, A. K., Sharma, U. K. & Sharma, N. A comprehensive review on vanilla flavor: extraction, isolation and quantification of vanillin and others constituents. *Int. J. Food Sci. Nutr.* **59**(4), 299–326 (2008).
149. Kwon, D. H. et al. Schisandrin A suppresses lipopolysaccharide-induced inflammation and oxidative stress in RAW 264.7 macrophages by suppressing the NF-κB, MAPKs and PI3K/Akt pathways and activating Nrf2/HO-1 signaling. *Int. J. Mol. Med.* **41**(1), 264–274 (2018).
150. Szopa, A. et al. Targeted lignan profiling and anti-inflammatory properties of Schisandra rubriflora and schisandra chinensis extracts. *Molecules* **23**(12) (2018).
151. Lee, H. J. et al. Paeonol oxime inhibits bFGF-induced angiogenesis and reduces VEGF levels in fibrosarcoma cells. *PLoS One*. **5**(8), e12358 (2010).
152. Singh, S., Bharti, N. & Mohapatra, P. P. Chemistry and biology of synthetic and naturally occurring antiamoebic agents. *Chem. Rev.* **109**(5), 1900–1947 (2009).
153. Trost, B. M., Silverman, S. M. & Stambuli, J. P. Palladium-catalyzed asymmetric [3 + 2] cycloaddition of trimethylenemethane with imines. *J. Am. Chem. Soc.* **129**(41), 12398–12399 (2007).
154. Parks, H. M. et al. Redirecting tropane alkaloid metabolism reveals pyrrolidine alkaloid diversity in Atropa belladonna. *New. Phytol.* **237**(5), 1810–1825 (2023).
155. Axente, R. E. et al. Application of ionic liquids as mobile phase additives for simultaneous analysis of nicotine and its metabolite cotinine in human plasma by HPLC-DAD. *Molecules* **28**(4) (2023).
156. Bradshaw, J. H. & Puntis, J. W. Taurolidine and catheter-related bloodstream infection: a systematic review of the literature. *J. Pediatr. Gastroenterol. Nutr.* **47**(2), 179–186 (2008).
157. Crnich, C. J. & Maki, D. G. The promise of novel technology for the prevention of intravascular device-related bloodstream infection. II. Long-term devices. *Clin. Infect. Dis.* **34**(10), 1362–1368 (2002).
158. Chong, C. Y. et al. Taurolidine-citrate lock solution for the prevention of central line-associated bloodstream infection in paediatric haematology-oncology and gastrointestinal failure patients with high baseline central-line associated bloodstream infection rates. *J. Paediatr. Child. Health*. **56**(1), 123–129 (2020).
159. Salehi, B. et al. Therapeutic potential of α- and β-Pinene: a miracle gift of Nature. *Biomolecules* **9**(11) (2019).
160. Tang, F. H. et al. Investigating novel genes potentially involved in endometrial adenocarcinoma using next-generation sequencing and bioinformatic approaches. *Int. J. Med. Sci.* **16**(10), 1338–1348 (2019).
161. Alaouna, M. et al. Exploring Water-Soluble South African Tulbaghia Violacea Harv Extract as a Therapeutic Approach for Triple-negative breast Cancer Metastasis. *Curr. Issues Mol. Biol.* **46**(10), 10806–10828 (2024).
162. Lyantagaye, S. L. Methyl-D-glucopyranoside from Tulbaghia violacea extract induces apoptosis in vitro in cancer cells. *Bangladesh J. Pharmacol.* **8**(2), 93–101 (2013).
163. Wei, R. J., Zhang, X. S. & He, D. L. Andrographolide sensitizes prostate cancer cells to TRAIL-induced apoptosis. *Asian J. Androl.* **20**(2), 200–204 (2018).
164. Rasheduzzaman, M., Yin, H. & Park, S. Y. Cardiac glycoside sensitized hepatocellular carcinoma cells to TRAIL via ROS generation, p38MAPK, mitochondrial transition, and autophagy mediation. *Mol. Carcinog.* **58**(11), 2040–2051 (2019).
165. Taraphdar, A. K., Roy, M. & Bhattacharya, R. Natural products as inducers of apoptosis: implication for cancer therapy and prevention. *Curr. Sci.* 1387–1396 (2001).
166. Liu, L. et al. Adaptive endoplasmic reticulum stress signalling via IRE1α–XBP1 preserves Self-Renewal of Haematopoietic and Pre-leukaemic Stem cells. *Nat. Cell Biol.* **21**(3), 328–337 (2019).
167. Osterlund, E. J. et al. Efficacy and specificity of inhibitors of BCL-2 family protein interactions assessed by affinity measurements in live cells. *Sci. Adv.* **8**(16), eabm7375 (2022).
168. Liu, H. et al. Plumbagin exhibits Genotoxicity and induces G2/M cell cycle arrest via ROS-mediated oxidative stress and activation of ATM-p53 signaling pathway in Hepatocellular cells. *Int. J. Mol. Sci.* **24**(7) (2023).
169. Pucci, B., Kasten, M. & Giordano, A. Cell cycle and apoptosis. *Neoplasia* **2**(4), 291–299 (2000).
170. Saldivar, J. C. et al. An intrinsic S/G(2) checkpoint enforced by ATR. *Science* **361**(6404), 806–810 (2018).
171. Smith, H. L. et al. DNA damage checkpoint kinases in cancer. *Expert Rev. Mol. Med.* **22**, e2 (2020).
172. Esposito, F. et al. Wee1 kinase: a potential target to overcome tumor resistance to therapy. **22**(19), 10689 (2021).
173. Domagala, P. et al. BRCA1/2-negative hereditary triple-negative breast cancers exhibit BRCAness. *Int. J. Cancer*. **140**(7), 1545–1550 (2017).
174. Butturini, E. et al. Tumor Dormancy and Interplay with hypoxic Tumor Microenvironment. *Int. J. Mol. Sci.* **20**(17), 4305 (2019).
175. Lim, E. et al. Sensitizing HR-proficient cancers to PARP inhibitors. *Mol. Cell. Oncol.* **4**(6), e1299272 (2017).
176. Lees-Miller, S. P., Beattie, T. L. & Tainer, J. A. Noncoding RNA joins Ku and DNA-PKcs for DNA-break resistance in breast cancer. *Nat. Struct. Mol. Biol.* **23**(6), 509–510 (2016).
177. Goh, J. J. H. et al. Transcriptomics indicate nuclear division and cell adhesion not recapitulated in MCF7 and MCF10A compared to luminal A breast tumours. *Sci. Rep.* **12**(1), 20902 (2022).
178. Shi, Y. et al. DAXX, as a tumor suppressor, impacts DNA damage repair and sensitizes BRCA-Proficient TNBC cells to PARP inhibitors. *Neoplasia* **21**(6), 533–544 (2019).
179. Baeva, E. et al. Polysaccharides from basidiocarps of cultivating mushroom Pleurotus Ostreatus: isolation and structural characterization. *Molecules* **24**(15), 2740 (2019).
180. Luparello, C. et al. Cytotoxic potential of the coelomic fluid extracted from the Sea Cucumber Holothuria tubulosa against Triple-negative MDA-MB231 breast Cancer cells. *Biology (Basel)* **8**(4) (2019).
181. Septaningsih, D. A. et al. Untargeted metabolomics using UHPLC-Q-Orbitrap HRMS for identifying cytotoxic compounds on MCF-7 breast cancer cells from Annona muricata Linn leaf extracts as potential anticancer agents. *Phytochem Anal.* **35**(6), 1418–1427 (2024).

182. Wiegmans, A. P. et al. Genome instability and pressure on non-homologous end joining drives chemotherapy resistance via a DNA repair crisis switch in triple negative breast cancer. *NAR Cancer*. **3**(2), zcab022 (2021).
183. Lonati, E. et al. Digested Cinnamon (Cinnamomum verum J. Presl) Bark Extract modulates Claudin-2 gene expression and Protein Levels under TNFα/IL-1β inflammatory stimulus. *Int. J. Mol. Sci.* **24**(11) (2023).
184. Guney Eskiler, G. The Interaction of PI3K inhibition with homologous recombination repair in Triple negative breast Cancer cells. *J. Pharm. Pharm. Sci.* **22**(1), 599–611 (2019).
185. Crozier, L. et al. Cell overgrowth during G1 arrest triggers an osmotic stress response and chronic p38 activation to promote cell cycle exit (2022).
186. Audeh, M. W. Novel treatment strategies in triple-negative breast cancer: specific role of poly(adenosine diphosphate-ribose) polymerase inhibition. *Pharmgenomics Pers. Med.* **7**, 307–316 (2014).
187. Wang, G. et al. Simvastatin induces cell cycle arrest and inhibits proliferation of bladder Cancer cells via PPARγ signalling pathway. *Sci. Rep.* **6**(1) (2016).
188. Chen, M. C. et al. Simvastatin inhibits Cell Proliferation and Migration in Human anaplastic thyroid Cancer. *Int. J. Mol. Sci.* **18**(12) (2017).
189. Wang, S. T. et al. Simvastatin-Induced cell cycle arrest through inhibition of STAT3/SKP2 Axis and activation of AMPK to promote P27 and P21 Accumulation in Hepatocellular Carcinoma cells. *Cell Death Dis.* **8**(2), e2626–e2626 (2017).
190. Liu, T. et al. Inhibitory effect of selenium on Esophagus Cancer cells and the related mechanism. *J. Nutr. Sci. Vitaminol (Tokyo).* **66**(5), 456–461 (2020).
191. Jarpe, M. B. et al. Anti-apoptotic versus pro-apoptotic signal transduction: checkpoints and stop signs along the road to death. *Oncogene* **17**(11 Reviews), 1475–1482 (1998).
192. Yogosawa, S. & Yoshida, K. Tumor suppressive role for kinases phosphorylating p53 in DNA damage-induced apoptosis. *Cancer Sci.* **109**(11), 3376–3382 (2018).
193. Wei, H. et al. Structural insight into the molecular mechanism of p53-mediated mitochondrial apoptosis. *Nat. Commun.* **12**(1), 2280 (2021).
194. Hao, Q. et al. The ARTS of p53-dependent mitochondrial apoptosis. *J. Mol. Cell. Biol.* **14**(10) (2023).
195. Wei, H. et al. Structures of p53/BCL-2 complex suggest a mechanism for p53 to antagonize BCL-2 activity. *Nat. Commun.* **14**(1), 4300 (2023).
196. Eymin, B. & Gazzeri, S. Role of cell cycle regulators in lung carcinogenesis. *Cell. Adh Migr.* **4**(1), 114–123 (2010).
197. Basu, S., Nurse, P. & Jones, A. W. *Core Control Principles of the Eukaryotic Cell Cycle* (2021).
198. Segurado, M. & Tercero, J. A. The S-phase checkpoint: targeting the replication fork. *Biol. Cell.* **101**(11), 617–627 (2009).
199. Patel, D. R. & Weiss, R. S. A tough row to hoe: when replication forks encounter DNA damage. *Biochem. Soc. Trans.* **46**(6), 1643–1651 (2018).
200. Qiu, S. et al. Replication fork reversal and Protection. *Front. Cell. Dev. Biol.* **9**, 670392 (2021).
201. Bugallo, A. et al. S-phase checkpoint prevents leading strand degradation from strand-associated nicks at stalled replication forks. *Nucleic Acids Res.* **52**(9), 5121–5137 (2024).
202. Juan, L. S. et al. DNA damage triggers squamous metaplasia in human lung and mammary cells via Mitotic checkpoints. *Cell. Death Discov.* **9**(1) (2023).
203. Guo, P. et al. FadA promotes DNA damage and progression of Fusobacterium Nucleatum-Induced Colorectal Cancer through Up-Regulation of Chk2. *J. Exp. Clin. Cancer Res.* **39**(1) (2020).
204. Lulli, M. et al. DNA damage response protein CHK2 regulates metabolism in Liver Cancer. *Cancer Res.* **81**(11), 2861–2873 (2021).
205. Mukherjee, C. et al. RIF1 promotes replication Fork Protection and efficient restart to maintain Genome Stability. *Nat. Commun.* **10**(1) (2019).
206. Tye, S., Ronson, G. E. & Morris, J. R. A fork in the road: where homologous recombination and stalled replication fork protection part ways. *Semin Cell. Dev. Biol.* **113**, 14–26 (2021).
207. Chen, R. & Wold, M. S. Replication protein A: single-stranded DNA's first responder: dynamic DNA-interactions allow replication protein A to direct single-strand DNA intermediates into different pathways for synthesis or repair. *Bioessays* **36**(12), 1156–1161 (2014).
208. Yates, L. A. et al. A structural and dynamic model for the assembly of replication protein A on single-stranded DNA. *Nat. Commun.* **9**(1), 5447 (2018).
209. Hiramoto, K. et al. DNA strand-breaking activity and mutagenicity of 2,3-dihydro-3,5-dihydroxy-6-methyl-4H-pyran-4-one (DDMP), a Maillard reaction product of glucose and glycine. *Mutat. Res.* **395**(1), 47–56 (1997).
210. Husain, K. et al. Farnesyl dimethyl chromanol targets colon cancer stem cells and prevents colorectal cancer metastasis. *Sci. Rep.* **11**(1), 2185 (2021).
211. Morel, K. L. et al. NF-κB blockade with oral administration of Dimethylaminoparthenolide (DMAPT), delays prostate Cancer Resistance to Androgen receptor (AR) inhibition and inhibits AR variants. *Mol. Cancer Res.* **19**(7), 1137–1145 (2021).
212. Ibrahim, O. H. M. et al. Azadirachta indica A. Juss fruit mesocarp and epicarp extracts induce antimicrobial and antiproliferative effects against Prostate (PC-3), breast (MCF-7), and colorectal adenocarcinoma (Caco-2) cancer cell lines through upregulation of proapoptotic genes. *Plants (Basel)* **11**(15) (2022).
213. Saraei, M., Hossienzadeh, R. & Jabbari, M. J. H. C. Synthesis of mono-and bis-1, 2, 3-triazole derivatives containing 4 H-pyran-4-one moiety by 1, 3-dipolar cycloaddition reaction. **21**(2), 103–107 (2015).
214. Saraei, M. et al. Novel Functionalized monomers based on Kojic Acid: Snythesis, characterization, polymerization and evalution of antimicrobial activity. *Designed Monomers Polym.* **20**(1), 325–331 (2016).
215. Audu, O. Y. et al. Synthesis, characterization, molecular structure, and computational studies on 4 (1H)-pyran-4-one and its derivatives. **1245**, 131077 (2021).
216. Teimuri-Mofrad, R. & Abrishami, F. J. A. A convenient method for the synthesis of hydroxymethyl and carboxaldehyde derivatives of 3, 5-diphenyl-4H-pyran-4-one. **14**, 20–26 (2007).
217. Afarinkia, K., Bearpark, M. J. & Ndibwami, A. Computational and experimental investigation of the diels-Alder cycloadditions of 4-chloro-2(H)-pyran-2-one. *J. Org. Chem.* **68**(19), 7158–7166 (2003).
218. Henrikson, J. C. et al. Reappraising the structures and distribution of metabolites from black aspergilli containing uncommon 2-benzyl-4H-pyran-4-one and 2-benzylpyridin-4(1H)-one systems. *J. Nat. Prod.* **74**(9), 1959–1964 (2011).
219. Afarinkia, K., Bearpark, M. J. & Ndibwami, A. An experimental and computational investigation of the diels-Alder cycloadditions of halogen-substituted 2(H)-pyran-2-ones. *J. Org. Chem.* **70**(4), 1122–1133 (2005).
220. Eroğlu, H. E., Koca, I. & Yıldırım, I. J. C. In vitro cytotoxic potential of newly synthesized furo [3, 2-c] pyran-4-one derivatives in cultured human lymphocytes. **63**, 407–413 (2011).
221. Aghaei, E. et al. Anti-proliferative effects of Hydroxytyrosol against breast Cancer cell lines through induction of apoptosis. *Gene Cell. Tissue* **10**(1) (2022).
222. Nasrollahzadeh, A. et al. Blockade of Nuclear Factor-Kb (NF-Kb) pathway using Bay 11-7082 enhances Arsenic Trioxide-Induced Antiproliferative Activity in U87 Glioblastoma cells. *Rep. Biochem. Mol. Biol.* **10**(4), 602–613 (2022).
223. Safwat, G., Soliman, E. S. M. & Mohamed, H. R. H. Induction of ROS mediated genomic instability, apoptosis and G0/G1 cell cycle arrest by erbium oxide nanoparticles in human hepatic Hep-G2 cancer cells. *Sci. Rep.* **12**(1), 16333 (2022).
224. Balka, K. R. et al. TBK1 and IKKε Act redundantly to Mediate STING-Induced NF-κB responses in myeloid cells. *Cell. Rep.* **31**(1), 107492 (2020).

225. Dimitrakopoulos, F. I. et al. The fire within: NF-κB involvement in non–small cell Lung Cancer. *Cancer Res.* **80**(19), 4025–4036 (2020).
226. Farhat, F. et al. Expressions of Nuclear factor-kappa B and peroxisome proliferator-activated receptor-Gamma Proportional with clinical staging of nasopharyngeal carcinoma. **9**(B), 1347–1351 (2021).
227. Al-Rashed, F. et al. LPS induces GM-CSF production by breast Cancer MDA-MB-231 cells via long-chain Acyl-CoA synthetase 1. *Molecules* **25**(20) (2020).
228. Wa, Q. et al. Ectopic expression of mir-532-3p suppresses bone metastasis of prostate Cancer cells via inactivating NF-κB signaling. *Mol. Ther. Oncolytics*. **17**, 267–277 (2020).
229. Khatri, B. et al. Whole genome resequencing of Arkansas Progressor and Regressor line chickens to identify SNPs Associated with Tumor Regression. *Genes* **9**(10), 512 (2018).
230. Howard, G. A. et al. Therapeutic effect of Y-27632 on Tumorigenesis and Cisplatin-Induced Peripheral sensory loss through RhoA–NF-κB. *Mol. Cancer Res.* **17**(9), 1910–1919 (2019).
231. Buhrmann, C. et al. Curcumin attenuates Environment-Derived Osteoarthritis by Sox9/NF-kB Signaling Axis. *Int. J. Mol. Sci.* **22**(14), 7645 (2021).
232. Amici, A. et al. Pyrimidine nucleotidases from human erythrocyte possess phosphotransferase activities specific for pyrimidine nucleotides. *FEBS Lett.* **419**(2–3), 263–267 (1997).
233. Zhang, J. et al. 3,3'-Diindolylmethane enhances fluorouracil sensitivity via inhibition of pyrimidine metabolism in colorectal cancer. *Metabolites* **12**(5) (2022).
234. Hiraoka, N. et al. Purine analog-like properties of bendamustine underlie rapid activation of DNA damage response and synergistic effects with pyrimidine analogues in lymphoid malignancies. *PLoS One*. **9**(3), e90675 (2014).
235. Balzarini, J. et al. Antiretrovirus activity of a novel class of acyclic pyrimidine nucleoside phosphonates. *Antimicrob. Agents Chemother.* **46**(7), 2185–2193 (2002).
236. Winter, E. et al. Antitumoral activity of a Trichloromethyl Pyrimidine Analogue: Molecular Cross-talk between intrinsic and extrinsic apoptosis. *Chem. Res. Toxicol.* **27**(6), 1040–1049 (2014).
237. Liu, L. C. et al. Contribution of personalized cyclin D1 genotype to triple negative breast cancer risk. *Biomed. (Taipei)*. **4**(1), 3 (2014).
238. Li, Z. et al. Inhibition of miRNA–34a promotes triple negative cancer cell proliferation by promoting glucose uptake. **18**(5), 3936–3942 (2019).
239. Mamoor, S. PGM2L1 expression associates with survival in triple negative breast cancer (2021).
240. Mamoor, S. Differential expression of tubulin alpha 4a in triple negative breast cancer (2022).
241. Zhao, Y. et al. α-Pinene inhibits human prostate Cancer Growth in a mouse xenograft model. *Chemotherapy* **63**(1), 1–7 (2018).
242. Xu, Q. et al. α-pinene regulates miR-221 and induces G(2)/M phase cell cycle arrest in human hepatocellular carcinoma cells. *Biosci. Rep.* **38**(6) (2018).
243. Nosalova, N. et al. Oxidative stress mediated by pyrrolidine SS13 is involved in autophagic cell death induction in colorectal cancer cells (2023).
244. Nosalova, N. et al. Involvement of both extrinsic and intrinsic apoptotic pathways in Tridecylpyrrolidine-Diol Derivative-Induced apoptosis in Vitro. *Int. J. Mol. Sci.* **24**(14) (2023).
245. Li, L. et al. Schisandrin B enhances doxorubicin-induced apoptosis of cancer cells but not normal cells. *Biochem. Pharmacol.* **71**(5), 584–595 (2006).
246. Sarin, N. et al. Cisplatin resistance in non-small cell lung cancer cells is associated with an abrogation of cisplatin-induced G2/M cell cycle arrest. *PLoS One*. **12**(7), e0181081 (2017).
247. Nishida, H. et al. Inhibition of ATR protein kinase activity by schisandrin B in DNA damage response. *Nucleic Acids Res.* **37**(17), 5678–5689 (2009).
248. Feliciano, A. et al. miR-99a reveals two novel oncogenic proteins E2F2 and EMR2 and represses stemness in lung cancer. *Cell. Death Dis.* **8**(10), e3141 (2017).
249. Zhu, L. et al. Schizandrin A can inhibit non–small cell lung cancer cell proliferation by inducing cell cycle arrest, apoptosis and autophagy. *Int. J. Mol. Med.* **48**(6) (2021).
250. Chen, J. The cell-cycle arrest and apoptotic functions of p53 in Tumor initiation and progression. *Cold Spring Harb Perspect. Med.* **6**(3), a026104 (2016).
251. Luo, Z. et al. Hyperthermia exposure induces apoptosis and inhibits proliferation in HCT116 cells by upregulating miR-34a and causing transcriptional activation of p53. *Exp. Ther. Med.* **14**(6), 5379–5386 (2017).
252. Liu, T. et al. Combinatorial effects of lapatinib and rapamycin in triple-negative breast cancer cells. *Mol. Cancer Ther.* **10**(8), 1460–1469 (2011).
253. Qi, Y. et al. Methylseleninic acid enhances paclitaxel efficacy for the treatment of triple-negative breast cancer. *PLoS One*. **7**(2), e31539 (2012).
254. Zhang, X. et al. Schizandrin protects H9c2 cells against lipopolysaccharide-induced injury by downregulating Smad3. *J. Biochem. Mol. Toxicol.* **33**(5), e22301 (2019).
255. Zhao, B. et al. Schizandrin B attenuates hypoxia/reoxygenation injury in H9c2 cells by activating the AMPK/Nrf2 signaling pathway. *Exp. Ther. Med.* **21**(3), 220 (2021).
256. Moon, P. D., Jeong, H. J. & Kim, H. M. Effects of Schizandrin on the expression of thymic stromal lymphopoietin in human mast cell line HMC-1. *Life Sci.* **91**(11–12), 384–388 (2012).
257. Yun, M. Y., Kim, N. S. & Choi, H. J. Topical application of cream containing enriched-schizandrin from Schisandra Chinensis fruit exert anti-photoaging efficacy in ultraviolet B-irradicated hairless mice (2022).
258. Jacobi, C. A. et al. [Peritoneal instillation of taurolidine and heparin for preventing intraperitoneal tumor growth and trocar metastases in laparoscopic operations in the rat model]. *Langenbecks Arch. Chir.* **382**(4 Suppl 1), S31–S36 (1997).
259. Jacobi, C. A. et al. Inhibition of peritoneal tumor cell growth and implantation in laparoscopic surgery in a rat model. *Am. J. Surg.* **174**(3), 359–363 (1997).
260. McCourt, M. et al. Taurolidine inhibits Tumor Cell Growth in Vitro and in vivo. *Ann. Surg. Oncol.* **7**(9), 685–691 (2000).
261. Opitz, I. et al. Taurolidine and Povidone-Iodine induce different types of cell death in Malignant Pleural Mesothelioma. *Lung Cancer*. **56**(3), 327–336 (2007).
262. Walters, D. K. et al. Taurolidine: a novel anti-neoplastic agent induces apoptosis of osteosarcoma cell lines. *Invest. New. Drugs.* **25**(4), 305–312 (2007).
263. Jafarian, H., Amanati, A. & Badiee, P. Antifungal activity of Taurolidine against Mucorales: an in vitro study on clinical isolates. *Curr. Med. Mycol.* **8**(1), 26–31 (2022).
264. Srivastava, R. N. et al. Taurine is a future biomolecule for potential health benefits: a review. **5**(1), 1–13 (2022).
265. Sun, B. S. et al. Taurolidine induces apoptosis of murine melanoma cells in vitro and in vivo by modulation of the Bcl-2 family proteins. *J. Surg. Oncol.* **96**(3), 241–248 (2007).
266. Tsai, K. D. et al. Cuminaldehyde from Cinnamomum Verum induces cell death through Targeting Topoisomerase 1 and 2 in human colorectal adenocarcinoma COLO 205 cells. *Nutrients* **8**(6), 318 (2016).
267. Zhao, J. J. I. J. S. Effects of CB2 receptor agonist JWH133 on Al242-Induced hippocampal neurons. **9**(06), 1–4 (2020).
268. Martínez-Reyes, I. et al. Cycle and mitochondrial membrane potential are necessary for Diverse Biological functions. *Mol. Cell.* **61**(2), 199–209 (2016).

269. Popovych, M. V. et al. Bioenergetic characteristics of the Murine Nemeth-Kellner Lymphoma cells exposed to Thiazole Derivative in Complex with Polymeric nanoparticles. *Ukrainian Biochem. J.* **94**(6), 30–36 (2023).
270. Liu, S. et al. Lipopolysaccharide induces mitochondrial oxidative stress and accelerates apoptosis by activating ROS/NF-κB in osteoarthritis chondrocytes (2022).
271. Reymick, O. O. et al. Cuminaldehyde downregulates folate metabolism and membrane proteins to inhibit growth of Penicillium digitatum in citrus fruit. **1**(1), 104–123 (2024).
272. Jo, A. et al. Oxime Derivative TFOBO promotes cell death by modulating reactive oxygen species and regulating NADPH oxidase activity in myeloid leukemia. *Sci. Rep.*, **12**(1) (2022).
273. Pawlak, A. et al. Methoxy-substituted Γ-Oxa-E-Lactones Derived from flavanones—comparison of their Anti-tumor activity in Vitro. *Molecules* **26**(20), 6295 (2021).
274. Sahu, B. et al. Synthesis, characterization, molecular docking and in vitro anticancer activity of 3-(4-methoxyphenyl)-5-substituted phenyl-2-pyrazoline-1-carbothioamide. **12**, 1648–1658 (2021).
275. Valdameri, G. et al. Investigation of Chalcones as selective inhibitors of the breast Cancer resistance protein: critical role of Methoxylation in both inhibition potency and cytotoxicity. *J. Med. Chem.* **55**(7), 3193–3200 (2012).
276. Park, E. J. et al. Vanillin suppresses cell motility by inhibiting STAT3-mediated HIF-1α mRNA expression in malignant melanoma cells. **18**(3), 532 (2017).
277. Chen, H. J. et al. Cervical cancer cell proliferation inhibition by vanillin oxime through HIF–1α expression inhibition, ERK1/2 and Akt protein down-regulation. *Acta Biochim. Pol.* **69**(1), 79–84 (2022).
278. Li, J. M. et al. Vanillin-Ameliorated Development of Azoxymethane/Dextran Sodium Sulfate-Induced Murine Colorectal Cancer: the involvement of Proteasome/Nuclear Factor-κB/Mitogen-Activated protein kinase pathways. *J. Agric. Food Chem.* **66**(22), 5563–5573 (2018).
279. Bezerra, D. P., Soares, A. K. & de Sousa, D. P. Overview of the role of vanillin on redox status and cancer development. *Oxid. Med. Cell Longev.* **2016**, 9734816 (2016).
280. Thaweboon, S., Thaweboon, B., C.J.K.E, M. & Sopavanit Candidal Adhesion to an oral Obturator PMMA Resin Incorporated with Vanillin. **942**: pp. 71–76. (2023).
281. Srinual, S., Chanvorachote, P. & Pongrakhananon, V. Suppression of cancer stem-like phenotypes in NCI-H460 lung cancer cells by vanillin through an akt-dependent pathway. *Int. J. Oncol.* **50**(4), 1341–1351 (2017).
282. Nguyen, H. et al. Structural Determinants of Substrate Recognition in the HAD Superfamily Member d-glycero- d- anno-Heptose-1,7-Bisphosphate Phosphatase (GmhB). *Biochemistry* **49**(6), 1082–1092 (2010)
283. Sun, Y. et al. Structure and genetics of the O-antigen of Cronobacter turicensis G3882 from a new serotype, C. turicensis O2, and identification of a serotype-specific gene. *FEMS Immunol. Med. Microbiol.* **66**(3), 323–333 (2012).
284. Clarion, L. et al. C-glycoside mimetics inhibit glioma stem cell proliferation, migration, and invasion. *J. Med. Chem.* **57**(20), 8293–8306 (2014).
285. Nejatie, A. et al. Kinetic and structural characterization of Sialidases (Kdnases) from ascomycete fungal pathogens. *ACS Chem. Biol.* **16**(11), 2632–2640 (2021).
286. Yoshida, F. et al. Synthesis of the Core oligosaccharides of Lipooligosaccharides from Campylobacter jejuni: A putative cause of Guillain-Barré Syndrome. *Chemistry* **25**(3), 796–805 (2019).
287. Ghosh, S. et al. Enhancement of anti-neoplastic effects of cuminaldehyde against breast cancer via mesoporous silica nanoparticle based targeted drug delivery system. *Life Sci.* **298**, 120525 (2022).
288. Sulák, O. et al. Burkholderia cenocepacia BC2L-C is a super lectin with dual specificity and proinflammatory activity. *PLoS Pathog.* **7**(9), e1002238 (2011).

Author contributions

MA: investigation, preparation of original draft; TM: reviewing; RK: reviewing; NCM: reviewing; AC: reviewing; TEL: reviewing; MR: investigation; RH: writing and final editing; CP: methodology, conceptualization; ZD: conceptualization, supervision and reviewing. All authors read and approved the manuscript.

Funding

This research was funded by the South African Medical Research Council (SAMRC) Grant Number 23108 and the National Research Foundation (NRF) Grant Number 138139.

Declarations

Competing interests

The authors declare no competing interests.

Additional information

Supplementary Information The online version contains supplementary material available at https://doi.org/10.1038/s41598-025-88417-2.

Correspondence and requests for materials should be addressed to R.H. or Z.D.